OPEN ACCESS Freely available online

PLOS ONE

A Crucial Role for CDC42 in Senescence-Associated Inflammation and Atherosclerosis

Takashi K. Ito[1], Masataka Yokoyama[1], Yohko Yoshida[4], Aika Nojima[1], Hidetoshi Kassai[2], Kengo Oishi[1], Sho Okada[1], Daisuke Kinoshita[1], Yoshio Kobayashi[1], Marcus Fruttiger[3], Atsu Aiba[2], Tohru Minamino[4,5]*

1 Department of Cardiovascular Science and Medicine, Chiba University Graduate School of Medicine, Chiba, Japan, **2** Center for Disease Biology and Integrative Medicine, Faculty of Medicine, The University of Tokyo, Tokyo, Japan, **3** Institute of Ophthalmology, University College London, London, United Kingdom, **4** Department of Cardiovascular Biology and Medicine, Niigata University Graduate School of Medical and Dental Sciences, Niigata, Japan, **5** PRESTO, Japan Science and Technology Agency, Saitama, Japan

Abstract

Risk factors for atherosclerosis accelerate the senescence of vascular endothelial cells and promote atherogenesis by inducing vascular inflammation. A hallmark of endothelial senescence is the persistent up-regulation of pro-inflammatory genes. We identified CDC42 signaling as a mediator of chronic inflammation associated with endothelial senescence. Inhibition of CDC42 or NF-κB signaling attenuated the sustained up-regulation of pro-inflammatory genes in senescent human endothelial cells. Endothelium-specific activation of the p53/p21 pathway, a key mediator of senescence, also resulted in up-regulation of pro-inflammatory molecules in mice, which was reversed by Cdc42 deletion in endothelial cells. Likewise, endothelial-specific deletion of Cdc42 significantly attenuated chronic inflammation and plaque formation in atherosclerotic mice. While inhibition of NF-κB suppressed the pro-inflammatory responses in acute inflammation, the influence of Cdc42 deletion was less marked. Knockdown of cdc-42 significantly down-regulated pro-inflammatory gene expression and restored the shortened lifespan to normal in mutant worms with enhanced inflammation. These findings indicate that the CDC42 pathway is critically involved in senescence-associated inflammation and could be a therapeutic target for chronic inflammation in patients with age-related diseases without compromising host defenses.

Citation: Ito TK, Yokoyama M, Yoshida Y, Nojima A, Kassai H, et al. (2014) A Crucial Role for CDC42 in Senescence-Associated Inflammation and Atherosclerosis. PLoS ONE 9(7): e102186. doi:10.1371/journal.pone.0102186

Editor: Masanori Aikawa, Brigham and Women's Hospital, Harvard Medical School, United States of America

Received November 29, 2013; **Accepted** June 16, 2014; **Published** July 24, 2014

Funding: This work was supported by grants from the Ministry of Education, Culture, Sports, Science and Technology (http://www.jsps.go.jp/english/e-grants/grants01.html), GCOE program at Chiba University(http://www.isrt-gcoe-chiba.jp/eng/), and Japan Prize Foundation (http://www.japanprize.jp/en/) (to TKI), and by a Grant-in-Aid for Scientific Research from the Ministry of Education, Culture, Sports, Science and Technology of Japan, and the grants from the Ono Medical Research Foundation(http://www.ono.co.jp/jp/zaidan/), the Uehara Memorial Foundation(http://www.ueharazaidan.or.jp/), the Daiichi-Sankyo Foundation of Life Science(http://www.ds-fdn.or.jp/), the NOVARTIS Foundation for the Promotion Science(http://novartisfound.or.jp/), the Japan Diabetes Foundation(http://www.j-df.or.jp/), the Mitsui Life Social Welfare Foundation(http://www.kousei-zigyodan.or.jp/), the Naito Foundation(https://www.naito-f.or.jp/en/), the Japanese Society of Anti-aging Medicine(http://www.anti-aging.gr.jp/english/), the Life Science Foundation of Japan(http://www.lifesci-found.com/), the SENSHIN Medical Research Foundtion (www.mt-pharma.co.jp/zaidan/index.html), the Takeda Science Foundation(http://www.takeda-sci.or.jp/), and the Mitsubishi Pharma Research Foundation(http://www.mitsubishi-zaidan.jp/)(to TM). The funders had no role in study design, data collection and analysis, decision to publish, or preparation of the manuscript.

Competing Interests: The authors have declared that no competing interests exist.

* Email: t_minamino@yahoo.co.jp

Introduction

Chronic inflammation is characterized by the long-term presence of immune cells in affected tissues and is associated with age-related diseases such as cancer, neurodegenerative disorders, and cardiovascular disease [1]. Interestingly, levels of pro-inflammatory cytokines are elevated in the endothelial cells [2] and serum [3] of older persons in the absence of disease. Thus, inflammation that accompanies the natural aging process may contribute to the onset of age-related diseases, which are responsible for most of the mortality in modern societies.

A possible link between inflammation and aging is cellular senescence [4], which is defined as irreversible growth arrest occurring after the accumulation of DNA damage response (DDR) such as activation of p53 [4,5], and is thought to be an important anticancer mechanism [6]. There is evidence that the number of senescent cells increases in various tissues with chronological aging [6]. An important feature shared by several types of senescent cells is persistent up-regulation of inflammatory molecules such as cytokines and adhesion molecules that recruit inflammatory cells [4,5]. The pro-inflammatory phenotype of senescent cells can be triggered by the DDR, leading to activation of NF-κB and stimulation of the production of inflammatory cytokines [4,7,8]. Pro-inflammatory signals emitted by senescent cells may help to prevent the development of cancer by leading to the elimination of cells with oncogenes, which have the potential to become malignant [9,10]. Conversely, however, senescence-associated chronic inflammation could also promote tumor progression [6,11], as well as other age-related changes such as cataract and osteoporosis [12], by disrupting cell function and tissue architecture.

Atherosclerosis is also an age-related chronic inflammatory disease [13]. In persons with atherosclerosis, chronic inflammation is mainly induced by sterile stimuli and it accelerates disease progression [13,14]. The initial step of the atherosclerotic process involves recruitment of inflammatory monocytes to dysfunctional

endothelial cells [13,15]. Senescent endothelial cells have been suggested to represent "dysfunctional endothelial cells" since they are specifically localized in the atherosclerotic lesions of patients and share many common features, including the pro-inflammatory phenotype that can induce sterile inflammation related to atherosclerosis, [4,5,16]. Although senescence of endothelial cells has been implicated in the process of atherogenesis, a specific role of senescent endothelial cells in chronic inflammation associated with atherosclerosis remains uncertain due to the lack of *in vivo* models. The molecular mechanisms underlying the pro-inflammatory phenotype in senescent endothelial cells also remain unclear.

Cdc42 is a member of the Rho GTPase family, which regulates the organization, polarity, and growth of the actin cytoskeleton of cells [17]. Cdc42 has been demonstrated to be a signal transduction convergence point for intracellular signaling networks that mediates multiple signaling pathways, including tyrosine kinase receptors, heterotrimeric G-protein coupled receptors, cytokine receptors, integrins, and responses to physical and chemical stresses [17]. Aberrant activation of Cdc42 has been suggested to contribute to various pathological states, such as carcinogenesis, cardiovascular disease, diabetes, and neuronal degenerative diseases [18]. Recent evidence has also suggested a potential role of CDC42 in stem cell senescence [19] and in the aging of organisms, including humans and mice [20,21]. In this study, we identified CDC42 as a crucial regulator of sterile inflammation induced by endothelial cell senescence. We demonstrated that deletion of *CDC42* in endothelial cells prevents chronic inflammation and plaque formation in a murine model of atherosclerosis. We also showed that knockdown of the *CDC42* pathway attenuates over-activation of innate immunity (the counterpart of inflammation) and extends the lifespan of worms, suggesting an important role of CDC42 in aging as well as in chronic inflammation.

Results

NF-κB regulates the expression of pro-inflammatory genes in senescent endothelial cells

To investigate the mechanistic link between endothelial cell senescence and chronic inflammation, we introduced a retroviral vector encoding a negative regulator of the cell cycle, either cyclin-dependent kinase inhibitor 1A (p21) or cyclin-dependent kinase inhibitor 2A (p16), into human endothelial cells. Introduction of p21 or p16 led to stable cell cycle arrest with enlargement of the size of the affected cells and an increase of senescence-associated β-galactosidase activity, both of which are hallmarks of cellular senescence, and this growth arrest persisted for at least 14 days after infection (data not shown). We confirmed that there was a marked increase in the expression of p21 and p16 by human endothelial cells after infection with each vector (Figure S1A). Introduction of p21 or p16 also led to the up-regulation of pro-inflammatory cytokines and adhesion molecules relevant to atherosclerosis [15], such as chemokine (C–C motif) ligand 2 (*CCL2*; also known as monocyte chemoattractant protein-1: MCP-1), E-selectin (*SELE*), and vascular cell adhesion molecule 1 (*VCAM1*), at 6 days after infection (Figure 1A and 1B). These molecules showed similar up-regulation in human endothelial cells undergoing replicative senescence (Figure 1C). Up-regulation of pro-inflammatory genes was accompanied by senescence in all cells that we tested derived from five different individuals (Figure 1A–C and data not shown), suggesting that genetic variation among individuals does not significantly affect the inflammatory response.

We next examined the influence of knockdown of various genes by siRNA on the sustained up-regulation of pro-inflammatory genes in senescent human endothelial cells. We selected approximately 200 genes that are thought to be related to cellular senescence, metabolism, morphology, or the immune response (Table S1), and we transduced 3 siRNA sets for each gene into human endothelial cells undergoing senescence at 6 days after introduction of p21 or p16. Expression of pro-inflammatory molecules was examined by real-time PCR after 72 hours. Consistent with the results of previous studies [4], transfection of senescent endothelial cells with siRNA targeting the NF-κB component *RELA* (p65) significantly down-regulated the expression of pro-inflammatory genes to normal levels (Figure 1D and Figure S1B), while the cells remained in growth arrest (data not shown). We also found that the NF-κB pathway was significantly activated in senescent endothelial cells (Figure 1E). Indeed, knockdown of any of the three subunits of IκB kinase (IKKα, β, or γ), a positive regulator of the NF-κB pathway, normalized the expression of pro-inflammatory genes in senescent endothelial cells (Figure 1D and Figure S1B). Other studies of senescent cells have shown that DDR components, such as ATM and checkpoint kinase 2 (CHEK2), activate the transcription of pro-inflammatory genes like IL-6 and IL-8 [7,8]. We examined six sets of siRNAs targeting *ATM* or *CHEK2* (Figure S1C), and found that inhibition of these molecules did not consistently decrease the expression of *CCL2*, *SELE*, or *VCAM1* (data not shown). The results suggest that the ATM-CHEK2 signaling pathway is not essential for regulation of these pro-inflammatory genes in senescent endothelial cells.

CDC42 regulates pro-inflammatory gene expression in senescent endothelial cells

Among genes unrelated to the canonical NF-κB pathway, we found that knockdown of the CDC42 pathway significantly reduced the senescence-associated increase of pro-inflammatory molecules (Figure 2A). CDC42 belongs to the small Rho GTPase family that regulates the organization of the cytoskeleton and membrane in relation to cell polarity, proliferation, and motility [18]. Knockdown of *CDC42* or *PAK2* (one of the downstream kinases) suppressed the up-regulation of inflammatory genes (Figure 2A and Figure S1B). siRNAs targeting these genes changed the cell morphologies of treated cells. However, the changes of the cell shape were inconsistent among the 3 siRNAs targeting the same gene while the cells remained growth arrested in all the siRNA-treated senescent cells (data not shown) suggesting that the morphological changes did not reflect the escape from cellular senescence. Knockdown of other family members such as Rho (*RHOA* and *RAC1*) and PAK (*PAK1*, *3* and *4*) had less effect than that of *CDC42* or *PAK2* (data not shown). Like the NF-κB pathway, both CDC42 and PAK2 were activated as cells underwent senescence (Figure 2B and 2C). To investigate the potential relationship between CDC42 and NF-κB, we introduced an active form of *CDC42* (*CDC42* V12) [22] into normal endothelial cells (Figure 2D–F) by retroviral infection. Activation of CDC42 led to a significant increase of the expression of *CCL2*, *SELE*, and *VCAM1* (Figure 2D). However, there was no alteration of the replicative lifespan of the cells (Figure 2E), suggesting that CDC42-induced up-regulation of pro-inflammatory genes was unrelated to cell cycle regulation. In addition, knockdown of the NF-κB pathway markedly inhibited the up-regulation of pro-inflammatory gene expression induced by active CDC42 (Figure 2F and Figure S2). Moreover, introduction of a dominant-negative form of CDC42 (CDC42 N17) [22] into p21-induced senescent endothelial cells significantly down-regulated

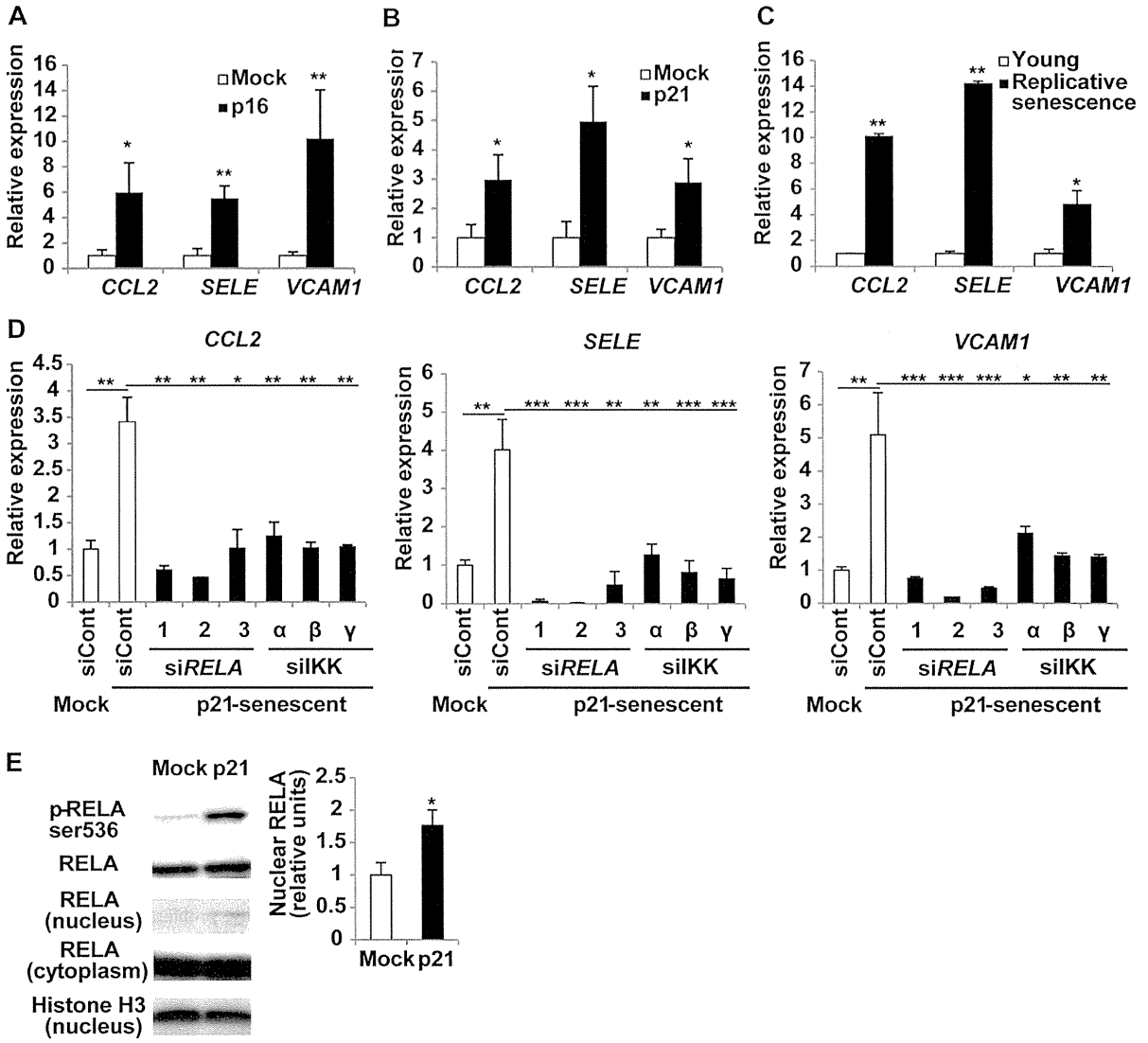

Figure 1. NF-κB signaling regulates pro-inflammatory gene expression in senescent endothelial cells. (A–C) Human endothelial cells were infected with an empty vector (Mock) or a retroviral vector encoding cyclin-dependent kinase inhibitor 1A (p21) or cyclin-dependent kinase inhibitor 2A (p16) to induce senescence. Expression of pro-inflammatory genes, such as the chemokine (C–C motif) ligand 2 (*CCL2*), E-selectin (*SELE*), and vascular cell adhesion molecule 1 (*VCAM1*), in senescent endothelial cells was examined by real-time PCR at 6 days after infection with the retroviral vector for p16 (A) or p21 (B) or after mock infection. Expression of pro-inflammatory genes was also examined in human endothelial cells undergoing replicative senescence (C). We defined cells with replicative senescence as cultures that did not show an increase in cell numbers and remained subconfluent for 2 weeks. n = 5. (D) Human endothelial cells were infected with an empty vector (Mock) or a retroviral vector encoding p21 to induce senescence (p21-senescent). Six days after infection, the cells were transduced with 3 sets of siRNAs for *RELA* (1–3), siRNAs for IKKs (α, β, γ subunits), or control siRNA (siCont). Expression of pro-inflammatory genes was examined by real-time PCR after 72 hours. n = 3. (E) Expression of RELA in the nuclear and cytoplasmic fractions and phospho-RELA in whole cell lysates was examined by western blotting at 6 days after retroviral infection. Samples were prepared as in Figure 1B. Histone H3 expression served as the internal control for nuclear extracts and the level of nuclear RELA relative to Histone H3 was quantified. n = 3. Data are shown as the mean ± SEM. *P<0.05, **P<0.01, ***P<0.001.
doi:10.1371/journal.pone.0102186.g001

NF-κB activity as well as the expression of pro-inflammatory genes (Figure 2G and H). These findings provide evidence that CDC42 up-regulates the expression of pro-inflammatory molecules in endothelial cells by activating the NF-κB pathway.

CDC42 regulates senescence-associated inflammation more specifically than NFκB

It is generally accepted that NF-κB is a crucial regulator of acute inflammation induced by infections [23,24]. To test whether the CDC42 pathway had a role in acute inflammation, we transfected normal endothelial cells with siRNA targeting *CDC42* before treating the cells with TNF-α or LPS (Figure 3A and 3B). In

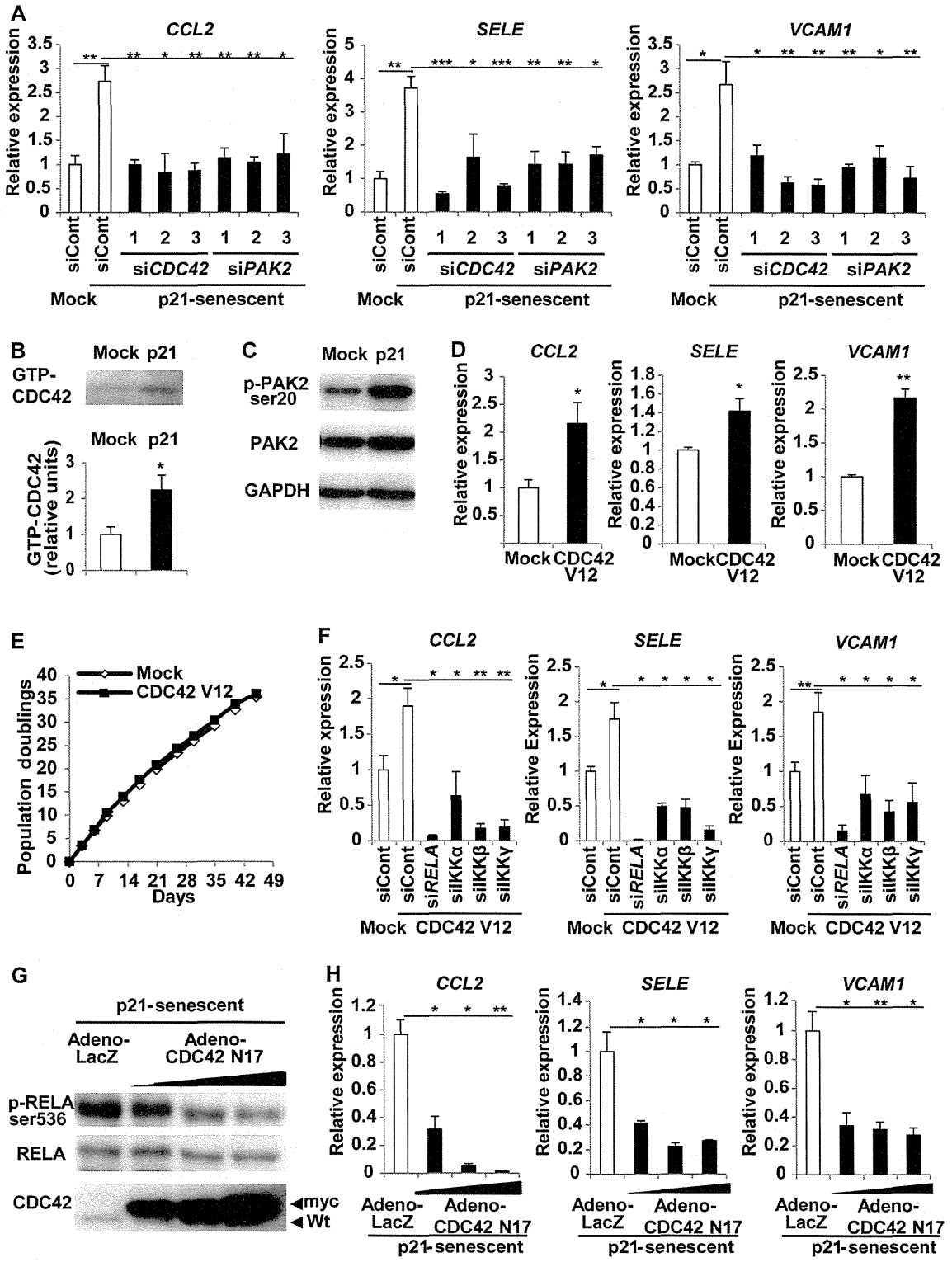

Figure 2. CDC42 signaling regulates pro-inflammatory gene expression in senescent endothelial cells. (A) Human endothelial cells were infected with an empty vector (Mock) or a retroviral vector encoding p21 to induce senescence (p21-senescent). Six days after infection, the cells were transduced with 3 sets of siRNAs for *CDC42*, siRNAs for *PAK2*, or control siRNA (siCont). Expression of pro-inflammatory genes was examined by

real-time PCR after 72 hours. n = 3. (B) Human endothelial cells were infected with an empty vector (Mock) or a retroviral vector encoding p21 to induce senescence (p21) and were harvested at 6 days after infection. The pull-down assay for active CDC42 (GTP-CDC42) was performed as described in Methods. The graph indicates the relative level of active CDC42. n = 3. (C) Expression of phopho-PAK2 and total PAK2 was examined by western blotting in human endothelial cells prepared as in Figure 2B. (D) Human endothelial cells were infected with an empty vector (Mock) or a retroviral vector encoding active CDC42 (CDC42 V12), and expression of pro-inflammatory genes was examined by real-time PCR at 6 days after infection. n = 3. (E) Proliferation of endothelial cells infected with a retroviral vector encoding active CDC42 (CDC42 V12) or an empty vector (Mock). n = 3. (F) Human endothelial cells were infected with an empty vector (Mock) or a retroviral vector encoding active CDC42 (CDC42 V12). Six days after infection, the cells were transduced with 3 sets of siRNAs for *RELA*, siRNA for IKKs, or control siRNA (siCont). Expression of pro-inflammatory genes was examined by real-time PCR after 72 hours. n = 3. (G) Human endothelial cells were infected with a retroviral vector encoding p21 to induce senescence (p21-senescent). Six days after retroviral infection, the cells were infected with an adenoviral vector encoding a dominant-negative form of myc-tagged CDC42 (CDC42 N17) or LacZ. Expression of phospho-RELA (Ser536) and total RELA were examined by western blotting at 48 hours after adenoviral infection. (H) Expression of pro-inflammatory genes in endothelial cells prepared as in Figure 2G was examined by real-time PCR. n = 3. Data are shown as the mean ± SEM. *P<0.05, **P<0.01, ***P<0.001.
doi:10.1371/journal.pone.0102186.g002

agreement with previous reports [23,24], knockdown of the NF-κB pathway markedly inhibited the up-regulation of pro-inflammatory molecules in response to stimulation with TNF-α or LPS (Figure 3A and B). In contrast, knockdown of *CDC42* or *PAK2* had a much weaker influence on the response to TNF-α (Figure 3A). Although the response to LPS was modestly attenuated in cells by CDC42 siRNA transfection, we still observed considerable production of inflammatory molecules, especially *SELE* (Figure 3B). Knockdown of siRNAs for *CDC42* or *PAK2* was no less efficient than that of NFκB (Figure 3C), which led us to assume that the differences in intervention for acute inflammatory induction was not merely due to the knockdown efficiency. These results suggest that CDC42 signaling in endothelial cells contributes more specifically to senescence-associated inflammation.

CDC42 promotes senescence-associated inflammation in mice

We next examined whether targeting *Cdc42* could inhibit senescence-associated inflammation *in vivo*. We established endothelium-specific *Mdm2* conditional knockout (CKO) mice (*Pdgfb*-Cre-ER; $Mdm2^{loxP/loxP}$). These mutant mice received intraperitoneal injections of tamoxifen once a day for five days from 6–8 weeks of age to induce Cre-mediated recombination and were analyzed after 3 weeks. Endothelial expression of Mdm2 (a negative regulator of p53 expression [25]) was abolished by treatment with tamoxifen, leading to up-regulation of the endothelial expression of p53 and p21, which are key indicators of cellular senescence. Nuclear staining for p53 and p21 was strong in the endothelial cells of most blood vessels in capillary-rich organs such as the lungs and the glomeruli of the kidneys (Figure 4A), while the endothelium of vessels in the liver was not stained for either p53 or p21 (data not shown), consistent with a previous report [26]. Immunohistochemistry also revealed an increase in the nuclear translocation of NF-κB (RelA) in *Mdm2* CKO mice (Figure 4A). We measured the expression of mRNA for p21 and pro-inflammatory genes in the lungs of *Mdm2* CKO mice after 3 weeks of tamoxifen treatment by real-time PCR. Consistent with the findings in senescent human endothelial cells, there was a marked increase of *CCL2* and *SELE* associated with up-regulation of p21 (Figure 4B). To further investigate the role of *Cdc42* in *Mdm2* CKO mice (*Pdgfb*-Cre-ER; $Mdm2^{loxP/loxP}$), we crossed floxed *Cdc42* mice ($Cdc42^{loxP/loxP}$) to obtain *Mdm2 Cdc42* CKO mice (*Pdgfb*-Cre-ER; $Mdm2^{loxP/loxP}$; $Cdc42^{loxP/loxP}$) and *Cdc42* CKO mice (*Pdgfb*-Cre-ER; $Cdc42^{loxP/loxP}$). As a result, we confirmed a decrease of *Cdc42* expression in the lungs of both *Cdc42* CKO mice and *Mdm2 Cdc42* CKO mice (Figure 4C). The inflammatory responses observed in *Mdm2* CKO mice was significantly attenuated in *Mdm2 Cdc42* CKO mice, whereas up-regulation of p21 was not affected by deletion of *Cdc42* (Figure 4B), suggesting that Cdc42 deletion inhibits p53-induced up-regulation of pro-inflammatory gene expression without having any influence on cell cycle regulation in this mouse model. *VCAM1* was not up-regulated in *Mdm2* CKO mice, unlike in senescent human endothelial cells, but was significantly decreased in double CKO mice compared with their littermates (Figure 4B). These results suggested that Cdc42 mediates p53-induced vascular inflammation in vivo.

To test whether endothelial cell Cdc42 deletion also inhibited chronic inflammation in a mouse model of atherosclerosis, we used apolipoprotein E knockout (*Apoe* KO) mice in which atherosclerotic plaque formation was enhanced by endothelial NF-κB signaling [27]. Accumulation of p21 proteins and senescence-associated β-galactosidase positive cells has also been reported in the aorta of this model [28]. Histological examination showed that nuclear expression of p21 was increased in the aortic endothelial cells of *Apoe* KO mice compared with wild-type mice (WT) (Figure 4D), supporting the notion that pro-senescence signaling is enhanced in the endothelium of atherosclerotic plaque. To investigate the role of Cdc42 in *Apoe* KO mice, we crossed endothelial cell-specific *Cdc42* CKO mice (*Pdgfb*-Cre-ER; $Cdc42^{loxP/loxP}$) with *Apoe* KO mice ($Apoe^{-/-}$) to establish Apoe KO Cdc42 CKO mice ($Apoe^{-/-}$; *Pdgfb*-Cre-ER; $Cdc42^{loxP/loxP}$). We then fed *Cdc42* CKO mice, their littermate controls (Cont), *Apoe* KO mice, and *Apoe* KO *Cdc42* CKO mice a high-cholesterol diet from 6–8 weeks of age and we simultaneously deleted endothelial *Cdc42* by treatment with tamoxifen. The aortic tissues were harvested for analysis of RNA and histological examination after 8 weeks (at 14–16 weeks old). To investigate the influence of *Cdc42* deletion on inflammation, we measured the expression of the macrophage surface marker *Cd68* by real-time PCR. The results showed that *Cd68* expression was markedly increased in *Apoe* KO mice, while this increase was significantly attenuated in *Apoe* KO *Cdc42* CKO mice (Figure 4E), suggesting that infiltration of macrophages into the aorta was significantly reduced by deletion of *Cdc42*. Up-regulation of pro-inflammatory genes in the aorta was also attenuated in *Apoe* KO *Cdc42* CKO mice compared with *Apoe* KO mice (Figure 4E). In contrast, expression of pro-inflammatory molecules did not differ between *Cdc42* CKO mice and their littermate controls (Figure 4E), suggesting that Cdc42 signaling was specifically activated by atherogenic stimuli, thereby provoking chronic inflammation. Aortic expression of p21 mRNA in *Apoe* KO mice was not altered by deletion of *Cdc42* (Figure 4E). Likewise, histological examination demonstrated that enhanced nuclear staining for p21 in the endothelial cells of *Apoe* KO mice was not attenuated by endothelial deletion of *Cdc42* (Figure 4F), indicating that ablation of Cdc42 did not affect cell cycle arrest. This conclusion was strengthened by the results of immunostaining for γ-H2AX, a marker of DNA damage and cellular senescence, since the

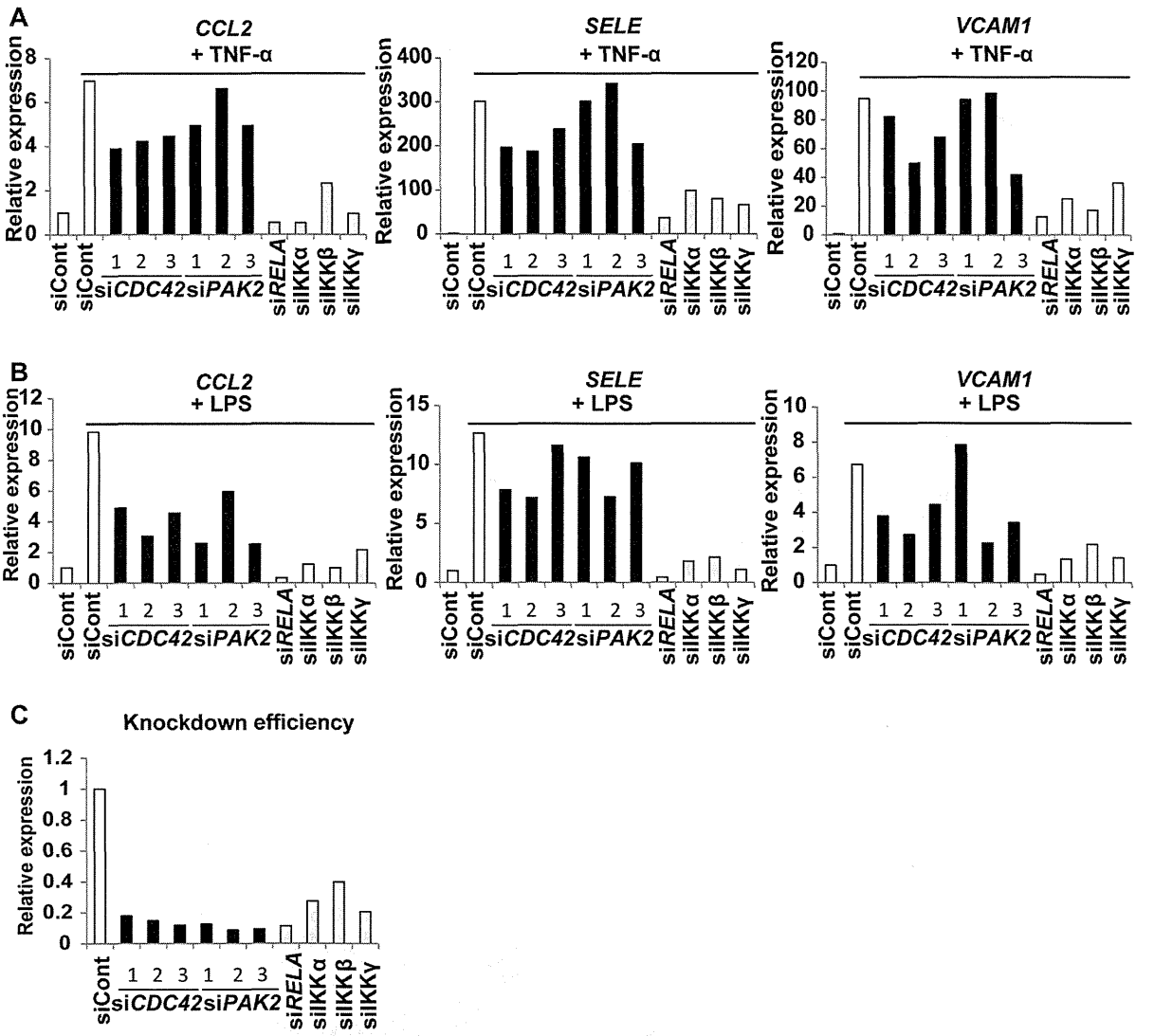

Figure 3. CDC42 signaling has a weaker influence on acute inflammation. (A and B) Human endothelial cells were transduced with siRNA for *CDC42*, *PAK2*, *RELA*, IKKs, or control siRNA (siCont). Cells were treated with TNF-α (A) or LPS (B) at 60 hours after siRNA transduction and were harvested 24 hours later to examine the expression of pro-inflammatory genes by real-time PCR. (C) Knockdown efficiency of siRNAs for *CDC42*, *PAK2*, and NFκB signaling in endothelial cells at 60 hours after transduction. The graph shows expression of each gene in siRNA-treated cells relative to that in siCont-treated cells. Each experiment in Figure 3A–C was repeated three times, and the results were consistent. Representative results are shown.
doi:10.1371/journal.pone.0102186.g003

expression of γ-H2AX was increased in the endothelium of *Apoe* KO mice and this increase was not affected by deletion of *Cdc42* (Figure S3). Thus, it is likely that atherogenic stimuli promote endothelial senescence and that Cdc42 is a mediator of chronic inflammation associated with endothelial senescence. We then further analyzed the influence of Cdc42 on the development of atherosclerosis. When cross-sections of the aortic sinus were stained with Oil red O to visualize atherosclerotic plaques, we found that the mean atherosclerotic lesion area was significantly smaller in *Apoe* KO *Cdc42* CKO mice than in their littermate controls (*Apoe* KO) (Figure 4G and H). These results suggested a crucial role of endothelial Cdc42 in chronic inflammation and the progression of atherosclerosis.

CDC42 promotes senescence-associated inflammation in worms

To further investigate the role of CDC42 in inflammation associated with senescence, we examined the influence of CDC42 deletion on aging and inflammation. The nematode *C. elegans* has recently been recognized as an excellent model for studying longevity and aging-associated phenotypes, mainly because of its short lifespan, availability of various genetic mutants, and amenability to genetic manipulation by RNA-interference (RNAi). We utilized *nol-6* mutant worms as a potential model of chronic inflammation that could mimic the phenotypic features of senescent human endothelial cells and *Apoe* KO mice, because this mutant displays over-activation of innate immunity (the

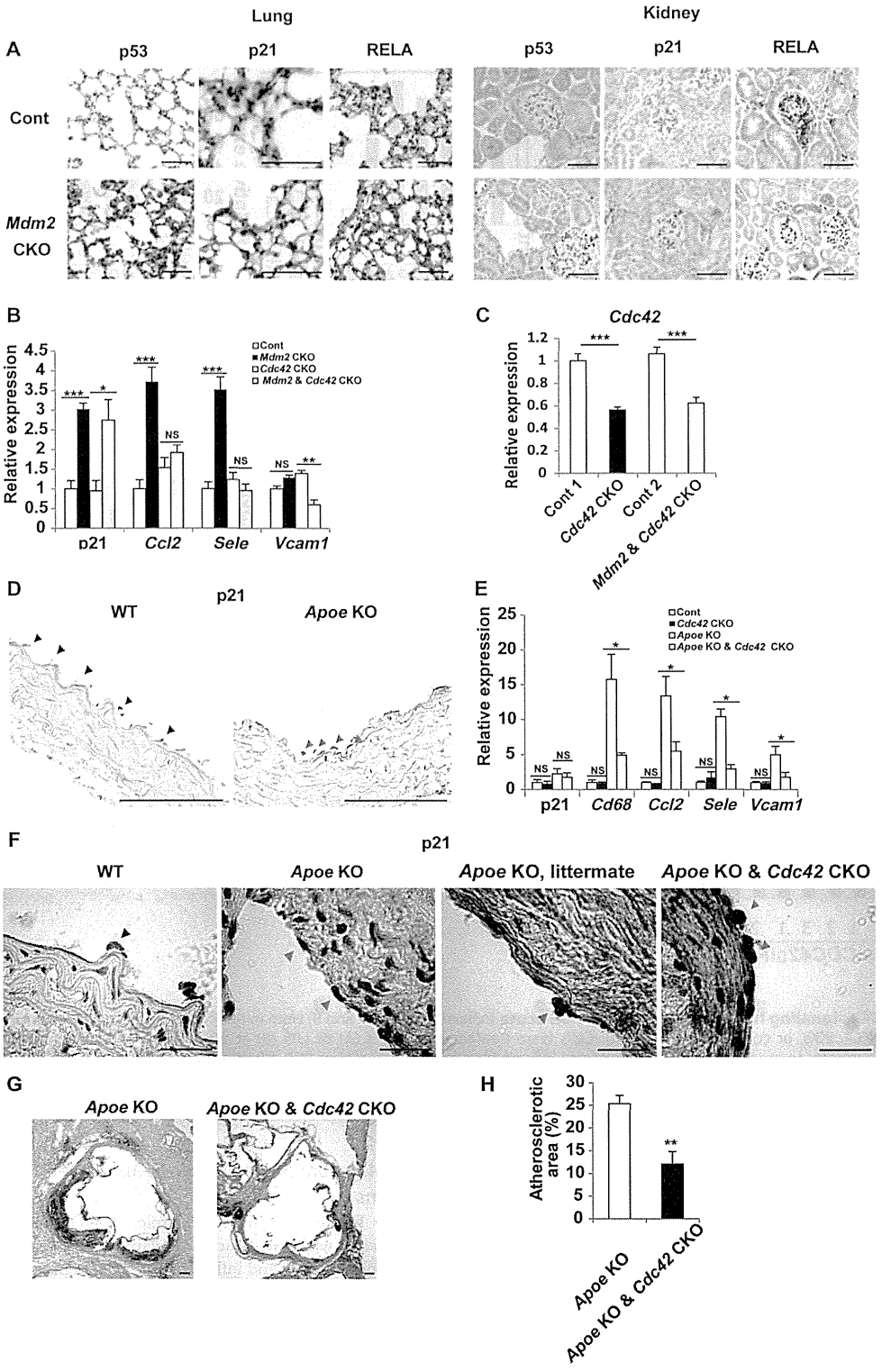

Figure 4. CDC42 signaling regulates chronic inflammation associated with senescence. (A) Immunostaining for p53, p21, and RELA in sections of the lungs and the renal glomeruli from endothelial cell-specific *Mdm2* conditional knockout mice (*Mdm2* CKO, *Pdgfb*-Cre-ER; $Mdm2^{loxP/loxP}$) and their littermate controls (Cont, $Mdm2^{loxP/loxP}$). Arrowheads indicate positive staining of capillary endothelial cells. Scale bar = 100 μm. (B) Expression of p21 and pro-inflammatory genes in the lungs of *Mdm2* CKO mice (*Pdgfb*-Cre-ER; $Mdm2^{loxP/loxP}$), their littermate controls (Cont,

Mdm2$^{loxP/loxP}$), *Cdc42* CKO mice (*Pdgfb*-Cre-ER; *Cdc42*$^{loxP/loxP}$), and *Mdm2* & *Cdc42* CKO mice (*Pdgfb*-Cre-ER; *Mdm2*$^{loxP/loxP}$; *Cdc42*$^{loxP/loxP}$) was examined by real-time PCR. n = 4–6. (C) Expression of *Cdc42* was examined by real-time PCR in the lungs of *Cdc42* CKO mice (*Pdgfb*-Cre-ER; *Cdc42*$^{loxP/loxP}$), their littermate controls (Cont 1, *Cdc42*$^{loxP/loxP}$), *Mdm2* & *Cdc42* CKO mice (*Pdgfb*-Cre-ER; *Mdm2*$^{loxP/loxP}$; *Cdc42*$^{loxP/loxP}$), and their littermate controls (Cont 2, *Mdm2*$^{loxP/loxP}$; *Cdc42*$^{loxP/loxP}$). n = 5–6. (D) Immunostaining for p21 in paraffin-embedded sections of the aorta from *Apoe* knockout mice (*Apoe* KO, *Apoe*$^{-/-}$) and wild-type littermates (WT, *Apoe*$^{+/+}$). Black arrowheads indicate negative staining of aortic endothelial cells. Red arrowheads indicate positive staining. Scale bar = 100 μm. (E) Expression of *Cdkn1a* (p21), *Cd68*, and pro-inflammatory genes in the aortas of *Cdc42* CKO mice (*Pdgfb*-Cre-ER; *Cdc42*$^{loxP/loxP}$), their littermate controls (Cont, *Cdc42*$^{loxP/loxP}$), *Apoe* KO mice (*Apoe*$^{-/-}$;*Cdc42*$^{loxP/loxP}$), and *Apoe* KO & *Cdc42* CKO mice (*Apoe*$^{-/-}$; *Pdgfb*-Cre-ER; *Cdc42*$^{loxP/loxP}$) was examined by real-time PCR. n = 4–6. (F) Immunostaining for p21 in frozen sections of the aorta from *Apoe* KO mice (*Apoe*$^{-/-}$), wild-type littermates (WT, *Apoe*$^{+/+}$), *Apoe* KO littermates (*Apoe*$^{-/-}$;*Cdc42*$^{loxP/loxP}$), and *Apoe* KO & *Cdc42* CKO mice (*Apoe*$^{-/-}$; *Pdgfb*-Cre-ER; *Cdc42*$^{loxP/loxP}$). Black arrowheads indicate negative staining of aortic endothelial cells for p21. Red arrowheads indicate positive staining for p21. Scale bar = 20 μm. (G) Oil red O staining of aortic sinus sections from *Apoe* KO mice (*Apoe*$^{-/-}$;*Cdc42*$^{loxP/loxP}$) and *Apoe* KO & *Cdc42* CKO mice (*Apoe*$^{-/-}$; *Pdgfb*-Cre-ER; *Cdc42*$^{loxP/loxP}$). Scale bar = 100 μm. (H) Quantification of the atherosclerotic lesion area relative to the total area at the level of the aortic sinus in *Apoe* KO mice and *Apoe* KO & *Cdc42* CKO mice. n = 5. Data are shown as the mean ± SEM. *P<0.05, **P<0.01, ***P<0.001.
doi:10.1371/journal.pone.0102186.g004

counterpart of inflammation) via a p53/cep-1-dependent pathway [29]. In this mutant, there was increased expression of inflammatory molecules such as *sym-1* (Figure 5A), as described previously [29], which is crucial for p53-dependent activation of innate immunity [29]. The lifespan of *nol-6* mutants raised at 22°C was significantly shorter than that of wild-type worms (Figure 5B), presumably due to the adverse influence of enhanced inflammation [29]. Knockdown of *cdc-42* or *max-2* (a homolog of *PAK2*) by feeding RNAi from the adult stage significantly down-regulated *sym-1* expression (Figure 5C and data not shown) and extended the lifespan of *nol-6* mutant worms to that of normal worms (Figure 5D and data not shown), further supporting a role of *cdc-42* in senescence-associated inflammation *in vivo*.

Discussion

The present findings provide evidence that the CDC42 pathway is critically involved in chronic inflammation induced by cellular aging signals. Inhibition of this pathway significantly attenuated the sustained up-regulation of inflammatory molecules in senescent human endothelial cells, as well as in murine models of cellular senescence and atherosclerosis, and in short-lived mutant worms. Thus, this inflammatory program appears to be conserved among species.

Despite evidence that accumulation of senescent endothelial cells occurs in atherosclerotic lesions and that senescent endothelial cells display the pro-inflammatory phenotype relevant to atherosclerosis [5,30], it has been unclear how senescence of endothelial cells influences the development of atherosclerosis. The present study identified CDC42 as a non-canonical pathway that activates NF-κB and up-regulates pro-inflammatory genes in senescent endothelial cells. We found that p53-induced vascular inflammation was significantly ameliorated by deletion of Cdc42 signaling. We also demonstrated that inhibition of Cdc42 signaling in the endothelium decreased vascular inflammation and plaque formation in a mouse model of atherosclerosis. It is interesting that deletion of CDC42 signaling had a much weaker influence on acute inflammation than chronic inflammation. Although the alleviated inflammation by Cdc42 deletion might also involve a declined response to exogenous ligands such as oxidized LDL [31], this work supports the notion that the Cdc42-dependet pro-inflammatory pathway is specifically activated by senescence-associated stimuli such as the risk factors for atherosclerosis.

Morphological change is one of the cardinal features of the senescent phenotype. It was reported that CDC42 was activated in senescent cells, contributing to morphological change [32]. Recently, CDC42 activation has also been implicated in the features of aging in mice and humans [20,21]. An age-associated increase of CDC42 contributes to the decline of hematopoietic stem cell function with aging [19]. It has been reported that disruption of Cdc42 GTPase-activating protein (Cdc42GAP), a negative regulator of Cdc42, leads to constitutive activation of CDC42 in various tissues of mice, as well as a premature aging-like phenotype and shortened lifespan [21]. In contrast to our *in vitro* experiments of endothelial cells, disruption of Cdc42GAP in mouse embryonic fibroblasts provoked premature senescence by activating p53 [21]. While CDC42 activation of NF-κB was also previously noted [33,34], CDC42 does not necessarily mediate NF-κB activation [33,35]. Thus, the role of CDC42 in inflammation and cellular senescence would be both cell type and context dependent.

Elimination of pre-senescent and senescent cells delays the onset of various age-related pathological conditions [12]. Our results suggested that inhibition of specific signaling in senescent cells is sufficient to ameliorate age-related diseases such as atherosclerosis. Because deletion of CDC42 had no effect on cell proliferation and only a weak influence on acute inflammation, CDC42 could be an attractive target for the treatment of age-associated diseases without promoting tumor formation or compromising normal immune function.

Methods

Cell culture, viral infection, and siRNA transfection

Human umbilical vein endothelial cells (HUVEC, Eidia) were maintained in EBM-2 (Lonza) supplemented with EGM-2 SingleQuots (Lonza) in dishes coated with gelatin (Sigma). In some experiments, LPS (1 μg/ml, Sigma) or TNF-α (2 ng/ml, eBioscience) was added to the culture medium and the cells were harvested for real-time PCR after 24 hours. Retroviral and adenoviral transduction was performed as described previously [36,37]. Briefly, cyclin-dependent kinase inhibitor 2A (p16) was cloned into the pBabe-puro retroviral vector and cyclin-dependent kinase inhibitor 1A (p21) and a constitutively active form of CDC42 (CDC42 V12) were cloned into the pLNCX vector. The respective empty vectors were used as controls. Retroviral stock solutions were supplemented with 8 μg/ml polybrene (Sigma, Tokyo, Japan) and cultured with HUVEC for 24 hours. Then infected cells were selected by culture for four days with 0.8 μg/ml puromycin for the pBabe-puro-based retroviral vector and with 500 μg/ml G418 for the pLNCN-based vectors. At six days after retroviral infection, siRNAs purchased from Ambion or Invitrogen were transfected at 10 nmol/L with RNAiFect (Qiagen) or Lipofectamine RNAiMAX (Invitrogen) according to the manufacturers' instructions. Cells were analyzed at 72 hours after transfection. The sequences of the siRNAs targeting CDC42 were UGGUGCUGUUGGUAAAACA, UGAGAUAACUCACCACUGU, and CAGUUAUGAUUGGUGGAGA; the sequences for PAK2 were GAACUGAUCAUUAACGAGA, GGUGAUGAAAGAAUUGAAA, and CAGAGGUGGUUACACGGAA; and the sequences for NF-κB signaling were CCCUUUACGUCAUCCCUGA, GGAGUACCCUGAGGCUAUA,

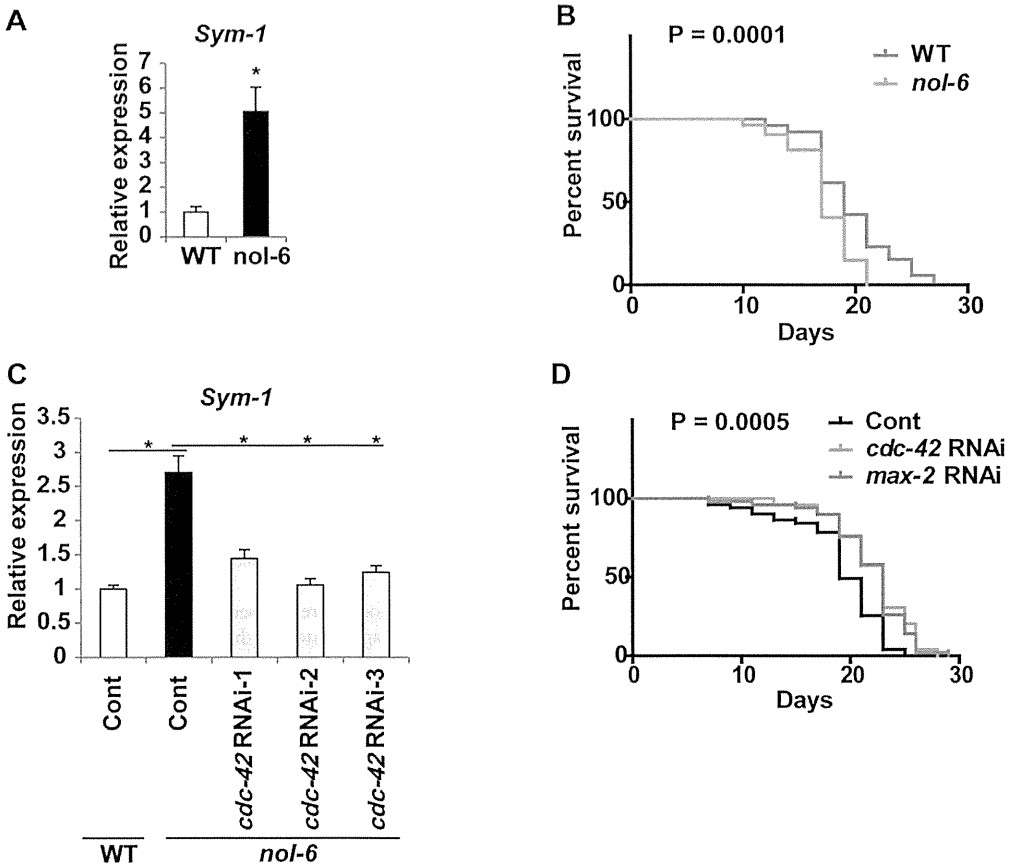

Figure 5. CDC42 promotes senescence-associated inflammation in worms. (A) Expression of *sym-1* in wild-type (WT) and *nol-6* mutant worms was examined by real-time PCR on day 9. n = 3. (B) Survival curves of wild-type (WT) and *nol-6* mutant worms maintained at 22°C. n = 50. (C) Expression of *sym-1* by wild-type (WT) and *nol-6* mutants treated with RNAi for *cdc-42* or control RNAi (Cont) was examined by real-time PCR. mRNA was analyzed 48 hours after starting feeding RNAi. n = 4. (D) Survival curves of *nol-6* mutant worms treated with RNAi for *cdc-42*, *max-2*, or control RNAi (Cont). n = 50. Data are shown as the mean ± SEM. *P<0.05, **P<0.01, ***P<0.001.
doi:10.1371/journal.pone.0102186.g005

GCCCUAUCCCUUUACGUCA (RELA), GGACUAAAAGAAGACUAUA (IKK-α), GACUUGAAUGGAACGGUGA (IKK-β), and GAUUGUGAUGGAGACCGUU (IKK-γ). High titer adenoviral stocks were generated with the Adeno-X Expression System (Clontech) according to the manufacturer's instructions. Infection was done for one hour with adenoviral stock solutions containing the dominant-negative form of CDC42, which were then replaced with normal culture medium.

Western blot analysis

Whole cell lysates were resolved by SDS polyacrylamide gel electrophoresis (PAGE). Proteins were transferred onto polyvinylidene difluoride (PVDF) membranes (Millipore) and were incubated with the primary antibody, followed by incubation with the specific horseradish peroxidase-conjugated immunoglobulin G antibody (anti-mouse, anti-rabbit, or anti- goat; Jackson). Specific proteins were detected by enhanced chemiluminescence (Amersham). Antibodies used for western blotting were as follows: anti-RELA antibody (Cell Signaling), anti-phospho-Ser536 RELA antibody (Cell Signaling), anti-PAK2 antibody (Cell Signaling), anti-phospho-ser20 PAK2 antibody (Cell Signaling), anti-CDC42 antibody (Cell Signaling), anti-histone H3 (Cell Signaling), and anti-GAPDH antibody (Santa Cruz). Nuclear and cytoplasmic extracts were prepared by using NE-PER nuclear and cytoplasmic extraction reagents (Pierce) to detect nuclear translocation of RELA. GTP-bound CDC42 was measured with the Active Cdc42 Pull-Down and Detection Kit (Thermo-Scientific). Briefly, whole cell lysates were prepared from human endothelial cells at 6 days after infection with pLNCX-p21 or pLNCX (Mock). The lysates were incubated with the GST-Pak1 binding domain fusion protein and glutathione resin to enable isolation of the target active (GTP-bound) GTPase. Unbound lysate proteins, including inactive or GDP-bound GTPase, were removed by using the spin columns and active GTPase was recovered from the glutathione resin by using SDS-PAGE loading buffer and analyzed by Western blotting. Then the immunoblot bands were quantified with Image J software.

Animal models

The animal study protocols were approved by the Chiba University Review Board and by the Committee on the Ethics of Animal Experiments of Chiba University (Permits Number: 21–254, 22–213, 23–88, 24–174, and 25–217). All mice were housed and maintained under pathogen-free conditions. Floxed *Cdc42*

mice (*Cdc42*$^{loxP/loxP}$), floxed *Mdm2* mice (*Mdm2*$^{loxP/loxP}$), and *Pdgfb*-Cre-ER mice were generated as described previously [26,38,39]. *Apoe* knockout mice were obtained from the Jackson Laboratory. The genetic background of floxed *Cdc42* mice was a hybrid of C57BL/6, ICR, and 129/Ola, while that of floxed *Mdm2* mice was a hybrid of C57BL/6, FVB, and 129S7/SvEvBrd, that of *Pdgfb*-Cre-ER mice was a hybrid of CBA and C57BL/6, and that of *Apoe* knockout mice was C57BL/6. Floxed *Mdm2* mice and *Pdgfb*-Cre-ER mice were backcrossed to C57BL/6 four times after being transferred to Chiba University. *Pdgfb*-Cre-ER mice were crossed with mice carrying floxed alleles to generate endothelial cell-specific gene knockout mice. In this model, the efficiency of tamoxifen-induced Cre recombinase activity has previously been tested with ROSA26-lacZ reporter mice, revealing that recombination was achieved in most of the endothelial cells of the capillaries and small arterioles in adult animals [26,40]. Although endogenous Pdgfb is also expressed by non-endothelial cells, it was previously demonstrated that transgene expression is endothelial cell-specific in various tissues including skeletal muscle, except for the liver [26]. We established endothelium-specific *Mdm2* conditional knockout (CKO) mice (*Pdgfb*-Cre-ER; *Mdm2*$^{loxP/loxP}$). To study the role of *Cdc42* in *Mdm2* CKO mice (*Pdgfb*-Cre-ER; *Mdm2*$^{loxP/loxP}$), we further crossed Cdc42 floxed mice (*Cdc42*$^{loxP/loxP}$) to obtain *Mdm2 Cdc42* CKO mice (*Pdgfb*-Cre-ER; *Mdm2*$^{loxP/loxP}$; *Cdc42*$^{loxP/loxP}$) and *Cdc42* CKO mice (*Pdgfb*-Cre-ER; *Cdc42*$^{loxP/loxP}$). These mutant mice received 4 mg of 4-hydroxytamoxifen (Sigma) intraperitoneally once a day for five days from 6–8 weeks of age to induce Cre-mediated recombination and were analyzed 3 weeks after treatment. Each experimental group was compared with their littermate controls. Before harvesting of tissue samples, mice were anesthetized with urethane (1 g/kg) and perfused with PBS. To study the role of *Cdc42* in *Apoe* knockout mice, we established *Apoe* KO *Cdc42* CKO mice (*Apoe*$^{-/-}$; *Pdgfb*-Cre-ER; *Cdc42*$^{loxP/loxP}$). *Apoe* KO mice (*Apoe*$^{-/-}$), their wild-type littermates (WT, *Apoe*$^{+/+}$), *Cdc42* CKO mice (*Pdgfb*-Cre-ER; *Cdc42*$^{loxP/loxP}$), their littermate controls (Cont, *Cdc42*$^{loxP/loxP}$), *Apoe* KO littermate mice (*Apoe*$^{-/-}$; *Cdc42*$^{loxP/loxP}$), and *Apoe* KO *Cdc42* CKO mice (*Apoe*$^{-/-}$; *Pdgfb*-Cre-ER; *Cdc42*$^{loxP/loxP}$) were fed a high-fat diet containing 1.25% cholesterol and 0.5% cholate (Oriental Kobo) from 6 to 8 weeks of age and then maintained for 8 weeks before analysis. Mice were killed by cervical dislocation and perfused with PBS. The aortas were dissected and cleaned of adherent connective tissue under a dissecting microscope. Then the proximal half of each aorta was homogenized for analysis of the expression of target markers.

Histological analysis

For immunohistochemistry, sections of paraffin-embedded or frozen tissues were incubated with antibodies for p53 (Vector Laboratories), p21 (BD Pharmingen and Abcam), RelA (Santa Cruz), and anti-γH2AX (Cell Signaling) after antigen retrieval by heating in citrate buffer. For analysis of atherosclerotic plaques in *Apoe* KO mice, 7 frozen cross-sections of the aortic sinus (10 μm thick) from each mouse were stained with Oil Red O (Sigma). Then the average lesion area was quantified with Image J software.

Worms

Bristol N2 wild-type and *nol-6* (AY1) strains were provided by Dr. Ishii and the Caenorhabditis Genetic Center, respectively. Temperature-sensitive *nol-6* mutants were maintained at 15°C. Lifespan experiments were performed at 22°C with 50 animals per condition. Synchronized L1 worms were fed with OP50. After the worms reached the young adult stage, FUdR (0.5 mg/ml) was added to the plate to prevent the production of progeny. On day 6, adult worms were placed on NGM plates containing IPTG (1 mmol/L) and carbenicillin (25 μg/ml) seeded with HT115 (DE3) bacteria carrying feeding RNAi plasmids or control L4440 vectors (Thermo-Scientific and DNAFORM). Survival was assessed every second or third day.

Real-time PCR

RNA was extracted from human cells, mouse tissues, or worms using RNABee (Tel-Test) and was transcribed to cDNA using a QuantiTect reverse transcription kit (Qiagen). Quantitative real-time PCR was performed with the Universal ProbeLibrary and a LightCycler 480 (Roche Applied Science). GAPDH was used to normalize the RNA content of human and mouse samples, while H20J04.3 [41] was applied for worm samples.

Statistical analysis

Data are shown as the mean ± SEM. The two-tailed Student's *t*-test or one way ANOVA was used to assess statistical significance (*P<0.05, **P<0.01, or ***P<0.001). For lifespan analysis of worms, the significance of differences was assessed by the log-rank (Mantel–Cox) test.

Supporting Information

Figure S1 Expression of cyclin-dependent kinases and knockdown efficacy in senescent human endothelial cells. (A) Human endothelial cells were infected with an empty vector (Mock) or a retroviral vector encoding cyclin-dependent kinase inhibitor 1A (p21) or cyclin-dependent kinase inhibitor 2A (p16) to induce senescence. Expression of p21 and p16 was examined by real-time PCR at 6 days after infection. Data are shown as the mean ± SEM. n = 5. (B) Human endothelial cells were infected with a retroviral vector encoding p21 to induce senescence. Six days after infection, the cells were transduced with 3 sets of siRNAs for *RELA* (1–3), siRNAs for IKKs (α, β, γ subunits), siRNAs for *Cdc42* (1–3), siRNAs for *PAK2* (1–3), or control siRNA (siCont). Expression of target genes was examined by real-time PCR after 72 hours. The graph shows expression of each gene in siRNA-treated cells relative to that in siCont-treated cells. Data are shown as the mean ± SEM. n = 3. (C) Human endothelial cells were infected with a retroviral vector encoding p21 to induce senescence. Six days after infection, the cells were transduced with 6 sets of siRNAs for *ATM* (1–6), siRNAs for *CHEK2* (1–6), or control siRNA (siCont). Expression of target genes was examined by real-time PCR after 72 hours. The graph shows expression of each gene in siRNA-treated cells relative to that in siCont-treated cells.
(DOCX)

Figure S2 Knockdown efficacy in human endothelial cells infected with active CDC42. Human endothelial cells were infected with a retroviral vector encoding active CDC42 (CDC42 V12). Six days after infection, the cells were transduced with siRNAs for *RELA*, IKKs (α, β, γ subunits), or control siRNA (siCont). Expression of the target genes was examined by real-time PCR after 72 hours. The graph shows expression of each gene in siRNA-treated cells relative to that in siCont-treated cells. Data are shown as the mean ± SEM. n = 3.
(DOCX)

Figure S3 Expression of γ-H2AX in the aorta. Immunostaining for γ-H2AX in sections of the aorta from *Apoe* KO mice (*Apoe*$^{-/-}$), wild-type littermates (WT, *Apoe*$^{+/+}$), *Apoe* KO

littermates (*Apoe*$^{-/-}$;*Cdc42*$^{loxP/loxP}$), and *Apoe* KO & *Cdc42* CKO mice (*Apoe*$^{-/-}$; *Pdgfb*-Cre-ER; *Cdc42*$^{loxP/loxP}$). Black arrowheads indicate negative staining of aortic endothelial cells for p21. Red arrowheads indicate positive staining for p21. Scale bar = 20 μm.
(DOCX)

Table S1 The gene list of siRNA screening.
(PDF)

Acknowledgments

We thank G. Lozano for floxed Mdm2 mice; T. Hayano for helping pathway screening with LC-MS/MS; I. Sakamoto, E. Takahashi, M. Iijima, E. Iiyama, T. Misawa, Y. Ishiyama and M. Kikuchi for technical support; Y. Shiraishi-Yamaguchi for CDC42 constructs; N. Ishii and R. Niwa for technical advice on C. elegans methods; Caenorhabditis Genetics Center (CGC) for C. elegans mutants.

Author Contributions

Conceived and designed the experiments: TKI TM. Performed the experiments: TKI MY YY AN HK KO SO DK. Analyzed the data: TKI YK TM. Contributed reagents/materials/analysis tools: HK MF AA. Wrote the paper: TKI TM.

References

1. Nathan C, Ding A (2010) Nonresolving inflammation. Cell 140: 871–882.
2. Donato AJ, Black AD, Jablonski KL, Gano LB, Seals DR (2008) Aging is associated with greater nuclear NF kappa B, reduced I kappa B alpha, and increased expression of proinflammatory cytokines in vascular endothelial cells of healthy humans. Aging Cell 7: 805–812.
3. Seidler S, Zimmermann HW, Bartneck M, Trautwein C, Tacke F (2010) Age-dependent alterations of monocyte subsets and monocyte-related chemokine pathways in healthy adults. BMC Immunol 11: 30.
4. Freund A, Orjalo AV, Desprez PY, Campisi J (2010) Inflammatory networks during cellular senescence: causes and consequences. Trends Mol Med 16: 238–246.
5. Minamino T, Komuro I (2007) Vascular cell senescence: contribution to atherosclerosis. Circ Res 100: 15–26.
6. Campisi J, Andersen JK, Kapahi P, Melov S (2011) Cellular senescence: a link between cancer and age-related degenerative disease? Semin Cancer Biol 21: 354–359.
7. Rodier F, Coppe JP, Patil CK, Hoeijmakers WA, Munoz DP, et al. (2009) Persistent DNA damage signalling triggers senescence-associated inflammatory cytokine secretion. Nat Cell Biol 11: 973–979.
8. Liu F, Wu S, Ren H, Gu J (2011) Klotho suppresses RIG-I-mediated senescence-associated inflammation. Nat Cell Biol 13: 254–262.
9. Kang TW, Yevsa T, Woller N, Hoenicke L, Wuestefeld T, et al. (2011) Senescence surveillance of pre-malignant hepatocytes limits liver cancer development. Nature 479: 547–551.
10. Lujambio A, Akkari L, Simon J, Grace D, Tschaharganeh DF, et al. (2013) Non-cell-autonomous tumor suppression by p53. Cell 153: 449–460.
11. Yoshimoto S, Loo TM, Atarashi K, Kanda H, Sato S, et al. (2013) Obesity-induced gut microbial metabolite promotes liver cancer through senescence secretome. Nature.
12. Baker DJ, Wijshake T, Tchkonia T, LeBrasseur NK, Childs BG, et al. (2011) Clearance of p16Ink4a-positive senescent cells delays ageing-associated disorders. Nature 479: 232–236.
13. Ross R (1999) Atherosclerosis–an inflammatory disease. N Engl J Med 340: 115–126.
14. Rock KL, Latz E, Ontiveros F, Kono H (2010) The sterile inflammatory response. Annu Rev Immunol 28: 321–342.
15. Libby P, Ridker PM, Maseri A (2002) Inflammation and atherosclerosis. Circulation 105: 1135–1143.
16. Minamino T, Komuro I (2008) Vascular aging: insights from studies on cellular senescence, stem cell aging, and progeroid syndromes. Nat Clin Pract Cardiovasc Med 5: 637–648.
17. Cerione RA (2004) Cdc42: new roads to travel. Trends Cell Biol 14: 127–132.
18. Sinha S, Yang W (2008) Cellular signaling for activation of Rho GTPase Cdc42. Cell Signal 20: 1927–1934.
19. Florian MC, Dorr K, Niebel A, Daria D, Schrezenmeier H, et al. (2012) Cdc42 activity regulates hematopoietic stem cell aging and rejuvenation. Cell Stem Cell 10: 520–530.
20. Kerber RA, O'Brien E, Cawthon RM (2009) Gene expression profiles associated with aging and mortality in humans. Aging Cell 8: 239–250.
21. Wang L, Yang L, Debidda M, Witte D, Zheng Y (2007) Cdc42 GTPase-activating protein deficiency promotes genomic instability and premature aging-like phenotypes. Proc Natl Acad Sci U S A 104: 1248–1253.
22. Luo L, Liao YJ, Jan LY, Jan YN (1994) Distinct morphogenetic functions of similar small GTPases: Drosophila Drac1 is involved in axonal outgrowth and myoblast fusion. Genes Dev 8: 1787–1802.
23. Li Q, Verma IM (2002) NF-kappaB regulation in the immune system. Nat Rev Immunol 2: 725–734.
24. Paludan SR (2000) Synergistic action of pro-inflammatory agents: cellular and molecular aspects. J Leukoc Biol 67: 18–25.
25. Brooks CL, Gu W (2006) p53 ubiquitination: Mdm2 and beyond. Mol Cell 21: 307–315.
26. Claxton S, Kostourou V, Jadeja S, Chambon P, Hodivala-Dilke K, et al. (2008) Efficient, inducible Cre-recombinase activation in vascular endothelium. Genesis 46: 74–80.
27. Garcus R, Kotsaki E, Xanthoulea S, van der Made I, Gijbels MJ, et al. (2008) Endothelial cell-specific NF-kappaB inhibition protects mice from atherosclerosis. Cell Metab 8: 372–383.
28. Kunieda T, Minamino T, Nishi J, Tateno K, Oyama T, et al. (2006) Angiotensin II induces premature senescence of vascular smooth muscle cells and accelerates the development of atherosclerosis via a p21-dependent pathway. Circulation 114: 953–960.
29. Fuhrman LE, Goel AK, Smith J, Shianna KV, Aballay A (2009) Nucleolar proteins suppress Caenorhabditis elegans innate immunity by inhibiting p53/CEP-1. PLoS Genet 5: e1000657.
30. Wang JC, Bennett M (2012) Aging and atherosclerosis: mechanisms, functional consequences, and potential therapeutics for cellular senescence. Circ Res 111: 245–259.
31. Choi SH, Harkewicz R, Lee JH, Boullier A, Almazan F, et al. (2009) Lipoprotein accumulation in macrophages via toll-like receptor-4-dependent fluid phase uptake. Circ Res 104: 1355–1363.
32. Cho KA, Ryu SJ, Oh YS, Park JH, Lee JW, et al. (2004) Morphological adjustment of senescent cells by modulating caveolin-1 status. J Biol Chem 279: 42270–42278.
33. Keestra AM, Winter MG, Auburger JJ, Frassle SP, Xavier MN, et al. (2013) Manipulation of small Rho GTPases is a pathogen-induced process detected by NOD1. Nature 496: 233–237.
34. Cammarano MS, Minden A (2001) Dbl and the Rho GTPases activate NF kappa B by I kappa B kinase (IKK)-dependent and IKK-independent pathways. J Biol Chem 276: 25876–25882.
35. Puls A, Eliopoulos AG, Nobes CD, Bridges T, Young LS, et al. (1999) Activation of the small GTPase Cdc42 by the inflammatory cytokines TNF(alpha) and IL-1, and by the Epstein-Barr virus transforming protein LMP1. J Cell Sci 112 (Pt 17): 2983–2992.
36. Miyauchi H, Minamino T, Tateno K, Kunieda T, Toko H, et al. (2004) Akt negatively regulates the in vitro lifespan of human endothelial cells via a p53/p21-dependent pathway. EMBO J 23: 212–220.
37. Aikawa R, Nagai T, Tanaka M, Zou Y, Ishihara T, et al. (2001) Reactive oxygen species in mechanical stress-induced cardiac hypertrophy. Biochem Biophys Res Commun 289: 901–907.
38. Aizawa R, Yamada A, Suzuki D, Iimura T, Kassai H, et al. (2012) Cdc42 is required for chondrogenesis and interdigital programmed cell death during limb development. Mech Dev 129: 38–50.
39. Grier JD, Xiong S, Elizondo-Fraire AC, Parant JM, Lozano G (2006) Tissue-specific differences of p53 inhibition by Mdm2 and Mdm4. Mol Cell Biol 26: 192–198.
40. Benedito R, Roca C, Sorensen I, Adams S, Gossler A, et al. (2009) The notch ligands Dll4 and Jagged1 have opposing effects on angiogenesis. Cell 137: 1124–1135.
41. Tan KT, Luo SC, Ho WZ, Lee YH (2011) Insulin/IGF-1 receptor signaling enhances biosynthetic activity and fat mobilization in the initial phase of starvation in adult male C. elegans. Cell Metab 14: 390–402.

Impact of Acute and Chronic Hyperglycemia on In-Hospital Outcomes of Patients With Acute Myocardial Infarction

Masashi Fujino, MD[a,b], Masaharu Ishihara, MD[c,*], Satoshi Honda, MD[a], Shoji Kawakami, MD[a], Takafumi Yamane, MD[a], Toshiyuki Nagai, MD[a], Kazuhiro Nakao, MD[a], Tomoaki Kanaya, MD[a], Leon Kumasaka, MD[a], Yasuhide Asaumi, MD[a], Tetsuo Arakawa, MD[a], Yoshio Tahara, MD[a], Michio Nakanishi, MD[a], Teruo Noguchi, MD[a], Kengo Kusano, MD[a,b], Toshihisa Anzai, MD[a,b], Yoichi Goto, MD[a], Satoshi Yasuda, MD[a,b], and Hisao Ogawa, MD[a,d]

This study was undertaken to assess the impact of acute hyperglycemia (acute-HG) and chronic hyperglycemia (chronic-HG) on short-term outcomes in patients with acute myocardial infarction (AMI). This study consisted of 696 patients with AMI. Acute-HG was defined as admission plasma glucose ≥200 mg/dl and chronic-HG as hemoglobin A1c ≥6.5%. Acute-HG was associated with higher peak serum creatine kinase (4,094 ± 4,594 vs 2,526 ± 2,227 IU/L, p <0.001) and in-hospital mortality (9.8% vs 1.6%, p <0.001). On the contrary, there was no significant difference in peak creatine kinase (2,803 ± 2,661 vs 2,940 ± 3,181 IU/L, p = 0.59) and mortality (3.3 vs 3.7%, p = 0.79) between patients with chronic-HG and those without. Multivariate analysis showed that admission plasma glucose was an independent predictor of in-hospital mortality (odds ratio 1.15, 95% confidence interval 1.05 to 1.27, p <0.001), but hemoglobin A1c was not. When only patients with acute-HG were analyzed, chronic-HG was associated with a significantly smaller infarct size (3,221 ± 3,001 vs 5,904 ± 6,473 IU/L, p <0.001) and lower in-hospital mortality (5.5 vs 18.9%, p = 0.01). In conclusion, these results suggested that acute-HG, but not chronic-HG, was associated with adverse short-term outcomes after AMI. Paradoxically, in patients with acute-HG, chronic-HG might abate the adverse effects of acute-HG. **(Am J Cardiol 2014;114:1789–1793)**

It has been reported that hyperglycemia (HG) causes oxidative stress, enhances inflammation, induces apoptosis, and activates coagulation, which deteriorate myocardial damage in the setting of ischemia.[1–3] In the clinical practice, admission plasma glucose is used as a measure of acute-HG and hemoglobin A1c (HbA1c) for chronic-HG. However, it remains unclear how acute-HG and chronic-HG affect short-term outcomes in patients with acute myocardial infarction (AMI). The purpose of the present study was to investigate impact of acute-HG and chronic-HG on short-term outcomes after AMI.

Methods

From January 2007 to June 2012, 760 consecutive patients who were admitted to National Cerebral and Cardiovascular Center of Japan within 48 hours after the onset of AMI were prospectively enrolled to the observational single-center registry and were retrospectively analyzed. In this registry, AMI was defined by a combination of 2 of the following 3: chest pain longer than 30 minutes, electrocardiographic signs, and elevation of serum creatine kinase more than twice the upper normal limit. Patients for whom laboratory data were lacking (n = 64) were excluded from the present study. Finally, this study consisted of the remaining 696 patients who constituted the study population with short-term clinical follow-up. The allocation of emergency coronary angiography and coronary intervention was determined by the physician's decision. The study protocol was approved by the Institutional Review Board of National Cerebral and Cardiovascular Center and was conducted in accordance with regulations governing epidemiological studies issued by the Ministry of Health, Labor, and Welfare of Japan.

On admission, age, gender, body mass index, and comorbidities such as hypertension, diabetes, dyslipidemia, smoker, and previous myocardial infarction were recorded. Plasma glucose was obtained at the time of admission, and HbA1c, during hospitalization. Serum creatine kinase was measured every 3 hours until it reached the peak value. Acute-HG was defined as admission plasma glucose ≥200 mg/dl.[4] Chronic-HG was defined as HbA1c ≥6.5%.[5] Chronic kidney disease is defined as estimated glomerular filtration rate ≤30 ml/min/1.73 m^2 in this study.

Continuous data were shown as mean ± SD. Continuous variables were compared by use of the *t* test and categorical

[a]Department of Cardiovascular Medicine, National Cerebral and Cardiovascular Center, Osaka, Japan; Departments of [b]Advanced Cardiovascular Medicine and [d]Cardiovascular Medicine, Graduate School of Medical Sciences, Kumamoto University, Kumamoto, Japan; and [c]Division of Coronary Heart Disease, Department of Internal Medicine, Hyogo College of Medicine, Nishinomiya, Japan. Manuscript received August 7, 2014; revised manuscript received and accepted September 17, 2014.

The present study was supported by the Intramural Research Fund, grant number 26-4-3, for Cardiovascular Diseases of the National Cerebral and Cardiovascular Center.

See page 1792 for disclosure information.

*Corresponding author: Tel: (+81) 798-45-6553; fax: (+81) 798-45-6551.

E-mail address: ishifami@fb3.so-net.ne.jp (M. Ishihara).

0002-9149/14/$ - see front matter © 2014 Elsevier Inc. All rights reserved.
http://dx.doi.org/10.1016/j.amjcard.2014.09.015

Table 1
Baseline characteristics of patients with and without acute hyperglycemia

Variables	Acute Hyperglycemia		p Value
	Yes (n=163)	No (n=533)	
Age (yrs)	68.7 ± 11.9	67.4 ± 12.8	0.268
Men	72%	72%	0.921
Body mass index (kg/m^2)	24.4 ± 3.8	23.3 ± 3.7	0.002
Diabetes Mellitus	69%	24%	<0.001
Hypertension	72%	66%	0.214
Dyslipidemia	61%	54%	0.105
Smoker	32%	33%	0.964
Chronic kidney disease	48%	29%	<0.001
Previous myocardial infarction	9%	10%	0.881
ST elevation myocardial infarction	80%	84%	0.342
Anterior location	39%	39%	1.000
Killip class 2 to 4	35%	14%	<0.001
Elapsed time (hour)	7.1 ± 10.2	7.5 ± 9.7	0.701
Primary percutaneous coronary intervention	90%	86%	0.349
Medication before infarction			
Antiplatelet agent	21%	18%	0.494
Angiotensin-converting enzyme inhibitors and/or angiotensin receptor blockers	31%	22%	0.021
Calcium-channel blocker	27%	26%	0.919
Beta-blocker	12%	10%	0.562
Statin	23%	17%	0.066
Oral hypoglycemic agent	29%	8%	<0.001
Insulin	9%	2%	<0.001

Table 2
Baseline characteristics of patients with and without chronic hyperglycemia

Variables	Chronic Hyperglycemia		p Value
	Yes (n=212)	No (n=484)	
Age (yrs)	68.6 ± 12.4	67.3 ± 12.7	0.192
Men	74%	71%	0.583
Body mass index (kg/m^2)	24.4 ± 3.9	23.2 ± 3.7	<0.001
Diabetes Mellitus	83%	13%	<0.001
Hypertension	73%	65%	0.065
Dyslipidemia	62%	53%	0.031
Smoker	34%	32%	0.736
Chronic kidney disease	36%	32%	0.296
Previous myocardial infarction	8%	10%	0.491
ST elevation myocardial infarction	80%	84%	0.229
Anterior location	36%	41%	0.238
Killip class 2 to 4	20%	19%	0.754
Elapsed time (hour)	8.1 ± 10.3	7.1 ± 9.6	0.206
Primary percutaneous coronary intervention	88%	87%	0.711
Medication before infarction			
Antiplatelet agent	20%	18%	0.600
Angiotensin-converting enzyme inhibitors and/or angiotensin receptor blockers	31%	21%	0.007
Calcium-channel blocker	27%	26%	0.926
Beta-blocker	10%	11%	1.000
Statin	22%	18%	0.090
Oral hypoglycemic agent	35%	4%	<0.001
Insulin	9%	1%	<0.001

variables with chi-square statistics or Fisher's exact test. Logistic regression analysis was used to obtain odds ratio (OR) and 95% confidence interval (CI) for in-hospital mortality. In multivariate analysis, the association between acute-HG and chronic-HG were adjusted for baseline variables, including age, gender, smoker, previous myocardial infarction, elapsed time, ST-elevation myocardial infarction, Killip classification ≥2, and primary coronary intervention. Multivariate analysis was also performed when plasma glucose and HbA1c were analyzed as a continuous variable. Values of $p < 0.05$ were considered statistically significant. All statistical analyses were performed using JMP (version 11.0, SAS Inc., Tokyo, Japan).

Results

This study consisted of 696 patients. A total of 652 patients (94%) underwent emergency coronary angiography. Primary coronary intervention was performed in 606 patients (87%), mostly with stents (92%). Final Thrombolysis In Myocardial Infarction grade 3 flow was obtained in 553 patients (91%).

Acute-HG was found in 163 patients (23%). Table 1 lists the baseline characteristics of patients with and without acute-HG. Patients with acute-HG had significantly higher plasma glucose on admission (276 ± 75 vs 139 ± 28 mg/dl, $p < 0.001$) and HbA1c (7.2 ± 1.9 vs 5.6 ± 0.8%, $p < 0.001$) than those without acute-HG. Acute-HG was associated with more diabetes, more chronic kidney disease, more Killip classification ≥2, and higher body mass index.

There were 212 (30%) patients with chronic-HG. The baseline characteristics of patients with chronic-HG and without chronic-HG were listed in Table 2. Both admission plasma glucose and HbA1c were higher in patients with chronic-HG than without chronic-HG (223 ± 86 vs 148 ± 52 mg/dl, $p < 0.001$ and 7.5 ± 1.5 vs 5.4 ± 0.3%, $p < 0.001$, respectively). Chronic-HG was associated with more diabetes and more dyslipidemia.

Peak creatine kinase was obtained in 691 patients (99%). Patients with acute-HG had a significantly higher peak creatine kinase than those without ($p < 0.001$; Figure 1). There was no significant difference in peak creatine kinase between patients with chronic-HG and those without ($p = 0.59$; Figure 1). In-hospital mortality rate was significantly higher in patients with acute-HG than in those without ($p < 0.001$; Figure 1), but chronic-HG was not associated with in-hospital mortality ($p = 0.79$; Figure 1).

In univariate analysis, acute-HG was associated with a sixfold increase in in-hospital mortality risk (OR 6.34, 95% CI 2.8 to 15.3, $p < 0.001$). When plasma glucose was analyzed as a continuous variable, an increase of 1 mmol/L (18 mg/dl) in plasma glucose was associated with an increase in mortality risk of 18% (OR 1.18, 95% CI 1.10

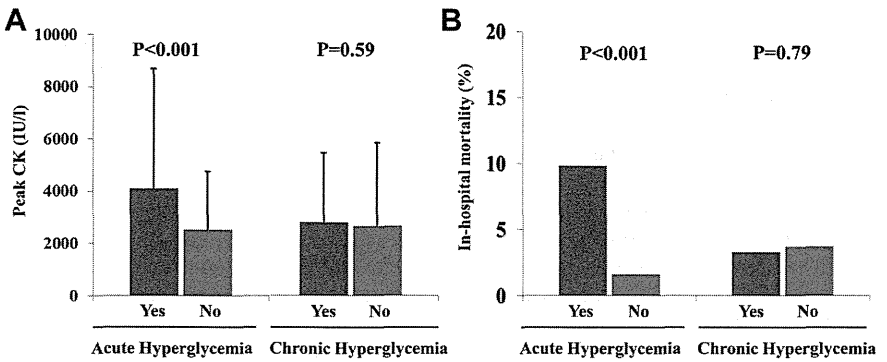

Figure 1. Effects of acute-HG and chronic-HG on peak creatine kinase and in-hospital mortality. *(A)* Patients with acute-HG had a significantly higher peak creatine kinase than those without (4,094 ± 4,594 vs 2,526 ± 2,227 IU/L, p <0.001). There was no significant difference in peak creatine kinase between patients with and without chronic-HG (2,803 ± 2,661 vs 2,940 ± 3,181 IU/L, p = 0.59). *(B)* In-hospital mortality rate was significantly higher in patients with acute-HG than in patients without (9.8% vs 1.6%, p <0.001). There was no significant difference in mortality between patients with and without chronic-HG (3.3 vs 3.7%, p = 0.79). CK = creatine kinase; HG = hyperglycemia.

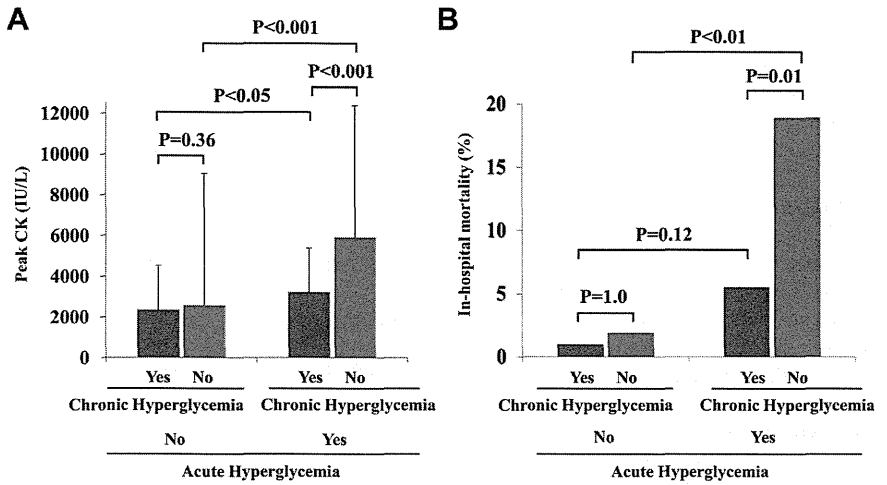

Figure 2. Effects of chronic-HG on peak creatine kinase and in-hospital mortality in patients with acute-HG and in those without acute-HG. (A) When only patients without acute-HG were analyzed, there was no significant difference in peak creatine kinase (2,348 ± 2,156 vs 2,572 ± 2,244 IU/L, p = 0.36) and in-hospital mortality (1.0 vs 1.9%, p = 1.00) between patients with and those without chronic-HG. (B) On the contrary, in patients with acute-HG, chronic-HG was associated with smaller peak creatine kinase (3,221 ± 3,001 vs 5,904 ± 6,473 IU/L, p <0.001) and lower mortality (5.5 vs 18.9%, p = 0.01). CK = creatine kinase; HG = hyperglycemia.

to 1.26, p <0.001). On the contrary, chronic-HG (OR 0.88, 95% CI 0.34 to 2.06, p = 0.79) and HbA1c (OR 1.14, 95% CI 0.85 to 1.43, p = 0.31) were not predictive factors of in-hospital mortality.

In multivariate analysis, acute-HG was independently associated with in-hospital mortality (OR 6.35, 95% CI 2.29 to 18.9, p <0.001), but chronic-HG was not (OR 0.47, 95% CI 0.15 to 1.37, p = 0.16). Analyzed as a continuous variable, plasma glucose was an independent predictor for in-hospital mortality (OR 1.21, 95% CI 1.09 to 1.35, p <0.001), but HbA1c was not (OR 0.85, 95% CI 0.57 to 1.20, p = 0.36).

Peak creatine kinase and in-hospital mortality are shown in Figure 2, stratified according to acute-HG and chronic-HG. Acute-HG was associated with large infarct size and high in-hospital mortality in both patients with and without chronic-HG. In 528 patients without acute-HG, there was no significant difference in peak creatine kinase and in-hospital mortality between patients with and without chronic-HG. On the contrary, in 163 patients with acute-HG, chronic-HG was associated with smaller peak creatine kinase and lower in-hospital mortality.

Discussion

The major findings of this study were (1) acute-HG was associated with large infarct size and high in-hospital mortality in patients with AMI, but chronic-HG was not and (2) in patients with acute-HG, chronic-HG was paradoxically associated with small infarct size and low mortality after AMI.

As previous studies have reported,[6–10] the present study showed that acute-HG is associated with larger infarct size and higher in-hospital mortality in patients with AMI. Although there had a been debate as to whether acute-HG is causally related to poor outcome after AMI or is simply an

epiphenomenon of the severe disease conditions, most recent studies have demonstrated that acute-HG is causally associated with further deterioration of myocardial damage and poor outcomes after reperfusion.

Acute-HG is observed not only in diabetic but also in nondiabetic patients with AMI. Although earlier studies classified nondiabetic patients with acute-HG as preexisting undiagnosed diabetes, recent studies have shown that acute-HG in nondiabetic patients does not represent preexisting undiagnosed diabetes.[11] In the thrombolysis era, it has been reported that diabetes and chronic glucose dysregulation, as assessed by HbA1c levels, are prognostic factors for in-hospital mortality in patients with AMI.[12] However, recent studies have shown that diabetes is not associated with short-term outcomes after AMI in patients who underwent primary coronary intervention.[9,13,14] In the present study, we also showed that chronic-HG assessed by HbA1c did not predict infarct size and in-hospital mortality in patients with AMI who were mostly treated with primary coronary intervention.

Several clinical and experimental studies have shown that acute increase of plasma glucose causes several unfavorable effects, including oxidative stress, inflammation, apoptosis, endothelial dysfunction, and hypercoagulation, that may contribute to the poor outcomes in patients with AMI. Esposito et al[1] reported that the plasma cytokine levels increased as the plasma glucose level increased during consecutive pulses of intravenous glucose but immediately returned to normal as plasma glucose returned to normal levels. Of note, when the first elevation in the blood glucose level was maintained by subsequent continuous intravenous glucose infusion, plasma cytokine concentrations gradually returned to normal levels, despite sustained high plasma glucose level. Apoptosis is also enhanced by intermittent, rather than constant, high glucose concentration.[2]

In patients with AMI who underwent primary coronary intervention, Iwakura et al[15] have shown that no-reflow phenomenon assessed by contrast echocardiography was predicted by acute-HG but not by a history of diabetes or by HbA1c. Recently, Teraguchi et al[16] reported, using continuous glucose measurement and cardiac magnetic resonance imaging, that there was a significant negative relation between glucose fluctuation and myocardial salvage index. In addition, we have previously reported that acute-HG abolishes ischemic preconditioning that has potent endogenous cardioprotective effect against myocardial ischemia.[17] These findings suggest that acute elevation of plasma glucose (acute-HG), but not constant high glucose concentration, deteriorates myocardial damage and outcomes after AMI.

In this study, we showed that acute-HG was associated with large infarct size and high in-hospital mortality in both patients with chronic-HG and those without. In patients without acute-HG, peak creatine kinase was small and mortality was low, regardless of the presence or absence of chronic-HG. Interestingly, chronic-HG was associated with small peak creatine kinase and low mortality in patients with acute-HG. There are several possible mechanisms that may explain this paradoxical finding. The magnitude of acute glucose elevation may become small in patients with chronic-HG because baseline glucose level should be high in these patients. Experimental studies have suggested that diabetic heart is paradoxically more resistant to ischemic insults. Decreased activity of sodium proton exchanger in diabetic myocardium may prevent reperfusion injury.[18] Also, decreased glucose utilization observed in diabetic cells may be beneficial in a circumstance of high plasma glucose.

Results of previous studies that have investigated whether continuous insulin infusion to normalize the glucose level will improve the outcome of patients with AMI are inconsistent.[19,20] Most of these studies consisted of patients with diabetes and/or acute-HG. Because impact of acute-HG is more pronounced in patients without chronic-HG, glucose control to correct acute-HG may be more beneficial for patients without chronic-HG or diabetes. Further studies should be warranted into the appropriate management in patients with AMI and acute-HG in the contemporary intervention era.

This study has the limitations of all retrospective investigations. However, this study consisted of consecutive patients with AMI who received contemporary management, including primary coronary intervention in 87% of patients. A small sample size is another limitation of this study. Because of the nature of observational study, the cause-effect relation between plasma glucose and outcomes and impact of acute management of plasma glucose on outcomes were not investigated.

Acknowledgment: We appreciate the assistance of our secretaries, Hiromi Maeda and Chieko Nagasawa.

Disclosures

The authors have no conflicts of interest to disclose.

1. Esposito K, Nappo F, Marfella R, Giugliano G, Giugliano F, Ciotola M, Quagliaro L, Ceriello A, Giugliano D. Inflammatory cytokine concentrations are acutely increased by hyperglycemia in humans: role of oxidative stress. *Circulation* 2002;106:2067–2072.
2. Risso A, Mercuri F, Quagliaro L, Damante G, Ceriello A. Intermittent high glucose enhances apoptosis in human umbilical vein endothelial cells in culture. *Am J Physiol Endocrinol Metab* 2001;281:E924–E930.
3. Stegenga ME, van der Crabben SN, Levi M, de Vos AF, Tanck MW, Sauerwein HP, van der Poll T. Hyperglycemia stimulates coagulation, whereas hyperinsulinemia impairs fibrinolysis in healthy humans. *Diabetes* 2006;55:1807–1812.
4. Sewdarsen M, Vythilingum S, Jialal I, Becker PJ. Prognostic importance of admission plasma glucose in diabetic and non-diabetic patients with acute myocardial infarction. *Q J Med* 1989;71:461–466.
5. Executive summary: standards of medical care in diabetes 2013. *Diabetes Care* 2013;36(Suppl 1):S4–S10.
6. Capes SE, Hunt D, Malmberg K, Gerstein HC. Stress hyperglycaemia and increased risk of death after myocardial infarction in patients with and without diabetes: a systematic overview. *Lancet* 2000;355:773–778.
7. Wahab NN, Cowden EA, Pearce NJ, Gardner MJ, Merry H, Cox JL. Is blood glucose an independent predictor of mortality in acute myocardial infarction in the thrombolytic era? *J Am Coll Cardiol* 2002;40:1748–1754.
8. Kosiborod M, Rathore SS, Inzucchi SE, Masoudi FA, Wang Y, Havranek EP, Krumholz HM. Admission glucose and mortality in elderly patients hospitalized with acute myocardial infarction: implications for patients with and without recognized diabetes. *Circulation* 2005;111:3078–3086.
9. Cao JJ, Hudson M, Jankowski M, Whitehouse F, Weaver WD. Relation of chronic and acute glycemic control on mortality in acute myocardial infarction with diabetes mellitus. *Am J Cardiol* 2005;96:183–186.

10. Ishihara M, Kojima S, Sakamoto T, Asada Y, Tei C, Kimura K, Miyazaki S, Sonoda M, Tsuchihashi K, Yamagishi M, Ikeda Y, Shirai M, Hiraoka H, Inoue T, Saito F, Ogawa H. Acute hyperglycemia is associated with adverse outcome after acute myocardial infarction in the coronary intervention era. *Am Heart J* 2005;150:814–820.
11. Ishihara M, Inoue I, Kawagoe T, Shimatani Y, Kurisu S, Hata T, Nakama Y, Kijima Y, Kagawa E. Is admission hyperglycaemia in non-diabetic patients with acute myocardial infarction a surrogate for previously undiagnosed abnormal glucose tolerance? *Eur Heart J* 2006;27:2413–2419.
12. Cakmak M, Cakmak N, Cetemen S, Tanriverdi H, Enc Y, Teskin O, Kilic ID. The value of admission glycosylated hemoglobin level in patients with acute myocardial infarction. *Can J Cardiol* 2008;24:375–378.
13. Britton KA, Aggarwal V, Chen AY, Alexander KP, Amsterdam E, Fraulo E, Muntner P, Thomas L, McGuire DK, Wiviott SD, Roe MT, Schubart UK, Fox CS. No association between hemoglobin A1c and in-hospital mortality in patients with diabetes and acute myocardial infarction. *Am Heart J* 2011;161:657–663.
14. Timmer JR, Hoekstra M, Nijsten MW, van der Horst IC, Ottervanger JP, Slingerland RJ, Dambrink JH, Bilo HJ, Zijlstra F, van't Hof AW. Prognostic value of admission glycosylated hemoglobin and glucose in nondiabetic patients with ST-segment-elevation myocardial infarction treated with percutaneous coronary intervention. *Circulation* 2011;124:704–711.
15. Iwakura K, Ito H, Ikushima M, Kawano S, Okamura A, Asano K, Kuroda T, Tanaka K, Masuyama T, Hori M, Fujii K. Association between hyperglycemia and the no-reflow phenomenon in patients with acute myocardial infarction. *J Am Coll Cardiol* 2003;41:1–7.
16. Teraguchi I, Imanishi T, Ozaki Y, Tanimoto T, Ueyama M, Orii M, Shiono Y, Shimamura K, Ishibashi K, Yamano T, Ino Y, Yamaguchi T, Hirata K, Kubo T, Sanke T, Akasaka T. Acute-phase glucose fluctuation is negatively correlated with myocardial salvage after acute myocardial infarction. *Circ J* 2013;78:170–179.
17. Ishihara M, Inoue I, Kawagoe T, Shimatani Y, Kurisu S, Nishioka K, Umemura T, Nakamura S, Yoshida M. Effect of acute hyperglycemia on the ischemic preconditioning effect of prodromal angina pectoris in patients with a first anterior wall acute myocardial infarction. *Am J Cardiol* 2003;92:288–291.
18. Ramasamy R, Schaefer S. Inhibition of Na+-H+ exchanger protects diabetic and non-diabetic hearts from ischemic injury: insight into altered susceptibility of diabetic hearts to ischemic injury. *J Mol Cell Cardiol* 1999;31:785–797.
19. Malmberg K, Rydén L, Efendic S, Herlitz J, Nicol P, Waldenström A, Wedel H, Welin L. Randomized trial of insulin-glucose infusion followed by subcutaneous insulin treatment in diabetic patients with acute myocardial infarction (DIGAMI study): effect on mortality at 1 year. *J Am Coll Cardiol* 1995;26:57–65.
20. The CREATE-ECLA trial group. Effect of glucose-insulin-potassium infusion on mortality in patients with acute ST-segment elevation myocardial infarction: the CREATE-ECLA randomized controlled trial. *JAMA* 2005;293:437–446.

Effect of Single Tibial Artery Revascularization on Microcirculation in the Setting of Critical Limb Ischemia

Osami Kawarada, MD; Satoshi Yasuda, MD, PhD; Kunihiro Nishimura, MD, PhD; Shingo Sakamoto, MD; Miyuki Noguchi, RN; Yasuomi Takahi, MD, PhD; Koichiro Harada, MD, PhD; Masaharu Ishihara, MD, PhD; Hisao Ogawa, MD, PhD

Background—Benefits of 2-dimensional (2D) angiosome-oriented infrapopliteal revascularization remain controversial. The aim of this retrospective study was to clarify the effect of single tibial artery revascularization on the dorsal and plantar microcirculation of critically ischemic limbs based on skin perfusion pressure (SPP).

Methods and Results—Fifty-seven interventions that only involved either anterior tibial artery (ATA) or posterior tibial artery (PTA) revascularization were included in this study. SPP was measured on the dorsal side (theoretically ATA perfusion area) and the plantar side (theoretically PTA perfusion area) before and after the procedure. Dorsal and plantar SPP increased significantly, from 33 (IQR 23–40.5) to 52 (IQR 32.5–65) mm Hg ($P<0.0001$) and 31.6±16.1 to 44.8±19.2 mm Hg ($P=0.001$) after ATA revascularization, respectively, and from 29.3±14.0 to 42.4±19.7 mm Hg ($P=0.003$) and 29.3±9.8 to 43.5±15.9 mm Hg ($P<0.001$) after PTA revascularization, respectively. Both ATA and PTA revascularization were not associated with any significant differences in ΔSPP between the dorsal and the plantar regions of the foot. Only 64% and 58% of ATA revascularization cases showed higher post-SPP and ΔSPP on the dorsal side than on the plantar side, respectively. Also, only 47% and 40% of PTA revascularization cases showed higher post-SPP and ΔSPP on the plantar side than on the dorsal side, respectively.

Conclusions—Single tibial artery revascularization, whether of the ATA or PTA, yielded comparable improvements in microcirculation of the dorsal and plantar foot. Approximately half of the feet revascularized had a change in microcirculation that was not consistent with the 2D angiosome theory. **(*Circ Cardiovasc Interv*. 2014;7:684-691.)**

Key Words: angioplasty ■ angiosome ■ microcirculation ■ peripheral arterial disease ■ reperfusion

The vascular community has been confused about the term angiosome because it relates to the treatment of infrapopliteal artery disease presenting as tissue loss. The original concept of the angiosome, introduced by Taylor and Palmer[1] in 1987 in the context of flaps for skin healing, is a 3-dimensional (3D) composite volume of skin, soft tissue, and bone supplied by a single source artery and its branches within the context of adjacent vascular territories. Each angiosome cannot be assessed after clamping or occlusion of adjacent source vessels and can be linked to its neighbors in all directions by either the true anastomoses without a change in caliber or by reduced-caliber choke arteries; therefore, the angiosome refers to the safe anatomic boundaries of tissue that can be transferred separately or combined together with source vessels as a composite flap.[1–6]

Editorial see p 642

Although even the original concept of the 3D angiosome might be less relevant to in vivo blood supply than to flap design,[7] the concept of a 2D angiosome as a uniform map of vascular territories with clear boundaries has emerged in the field of surgical and endovascular treatment for critical limb ischemia (CLI) with the past 5 years.[8–10] With this recent 2D angiosome concept, emphasis was placed on direct intervention, that is, revascularization of the artery feeding the 2D angiosome where ischemic ulcers or gangrene exist, instead of indirect intervention. However, currently there are active ongoing debates over the benefits of angiosome-oriented infrapopliteal revascularization in terms of clinical outcomes.[11–13]

Hence, objective evaluation of the circulation of the foot is essential for determining whether direct or indirect intervention is superior. Apart from the location of the wound, we simply define direct revascularization as revascularization of anterior tibial artery (ATA) system for dorsal foot circulation and revascularization of posterior tibial artery (PTA) system for plantar foot circulation and indirect revascularization as revascularization of PTA system for dorsal foot circulation and revascularization of ATA system for plantar foot circulation. The aim of this study was to investigate the effect of single tibial artery

Received December 30, 2013; accepted July 24, 2014.

From the Departments of Cardiovascular Medicine (O.K., S.Y., S.S., K.H., M.I., H.O.) and Preventive Medicine and Epidemiological Informatics (K.N.), National Cerebral and Cardiovascular Center, Osaka, Japan; Department of Advanced Cardiovascular Medicine (O.K., S.Y., M.I.) and Department of Cardiovascular Medicine (H.O.), Graduate School of Medical Sciences, Kumamoto University, Kumamoto, Japan; and Department of Cardiovascular Medicine, Nishinokyo Hospital, Nara, Japan (M.N., Y.T.).

Correspondence to Osami Kawarada, MD, Department of Cardiovascular Medicine, National Cerebral and Cardiovascular Center, 5-7-1 Fujishiro-dai, Suita, Osaka 565–8565, Japan. E-mail kawarada.osami.hp@ncvc.go.jp

Circ Cardiovasc Interv **is available at http://circinterventions.ahajournals.org** **DOI: 10.1161/CIRCINTERVENTIONS.113.001311**

WHAT IS KNOWN

- The original angiosome concept is a 3-dimensional (3D) volume of tissue supplied by a source artery.
- Recently, a 2D angiosome map has emerged in the treatment of symptomatic infrapopliteal artery disease.
- There is debate over the benefits of the 2D angiosome-oriented infrapopliteal revascularization in terms of clinical outcomes.

WHAT THE STUDY ADDS

- Irrespective of the 2D angiosome theory, single tibial artery revascularization resulted in comparable improvements in microcirculation of the dorsal and plantar foot.
- Approximately half of the feet undergoing single tibial artery revascularization presented a change in microcirculation that was not consistent with the 2D angiosome theory.

revascularization on the dorsal and plantar microcirculation of the foot to clarify the validity of the recent 2D angiosome in the treatment of symptomatic infrapopliteal artery disease.

Methods

Subjects

This retrospective study included a total of 108 infrapopliteal artery interventions performed for the treatment of CLI with tissue loss in 2 vascular centers between May 2011 and October 2013. Noninvasive evaluation of the microcirculation using skin perfusion pressure (SPP) was performed sequentially before the procedure and on the day after the procedure (or within 7 days in cases of measurement failure). The SPP measurements were available in 79 cases. Of them, the 57 interventions that only involved revascularization of either ATA or PTA were included (Figure 1). The study was approved by the institutional review committee.

SPP Measurement

Currently, SPP is available for the evaluation of microcirculation on the dorsal (ATA territory based on the recent definition of the angiosome) and plantar (PTA territory based on the recent definition of the angiosome) sides even in the setting of CLI.[14–18] The basic technique for measuring SPP was based on a previous study.[14] After each patient was placed in a supine position in a room maintained at room temperature between 24°C and 26°C, SPP was measured using a SensiLase PAD 3000 device (Vasamed, Inc, Eden Prairie, MN). A laser Doppler probe was placed under an 8.0-cm-wide blood pressure cuff wrapped around the middle of the first and second metatarsals on the dorsal and plantar aspects of the foot. SPP denotes the cuff pressure at which microcirculatory perfusion is first detected after a period of occlusion.

Statistical Analysis

Data are expressed as mean±SD, numbers with percentages, or medians and interquartile ranges. The normality of the distribution of continuous variables was determined using the Shapiro–Wilk test. Comparisons of the data before and after the procedure were analyzed using the paired t test for normally distributed variables and Wilcoxon signed-rank test for non-normally distributed variables, respectively. Comparisons of independent 2 groups were evaluated using Student t test for parametric variables and Mann–Whitney U test for nonparametric variables. Categorical variables were analyzed using either Pearson χ^2 test or Fisher exact test. P values <0.05 were considered significant. Corrections of multiple comparisons were made according to Bonferroni. Because some patients underwent several interventions, we conducted mixed model analysis using patient ID as a random intercept to adjust for autocorrelation using the xtmixed command in STATA. SPSS version 11.0 (SPSS Inc, Chicago, IL) and STATA version 13 (Stata Corp, College Station, TX) were used for statistical analyses.

Results

Baseline clinical characteristics of the study subjects are shown in Table 1. The breakdown of treated vessels is shown in Table 2. The distributions of SPP before and after ATA and PTA revascularization are shown in Figure 2. The number of final run-off vessels, as well as the number of limbs with a patent peroneal artery or pedal arch after ATA and PTA revascularization, are shown in Table 3.

With ATA revascularization, dorsal SPP increased significantly from 33 (IQR 23–40.5) to 52 (IQR 32.5–65) mm Hg (P<0.0001) after direct intervention and plantar SPP increased significantly from 31.6±16.1 to 44.8±19.2 mm Hg (P=0.001) after indirect intervention (Table 4). Also, there were no significant differences in both pre-SPP and post-SPP between the dorsal (direct intervention) side and the plantar (indirect intervention) side. ΔSPP was comparable between the dorsal (direct intervention) side and the plantar (indirect intervention) side (15.5±18.6 versus 13.2±21.3 mm Hg;

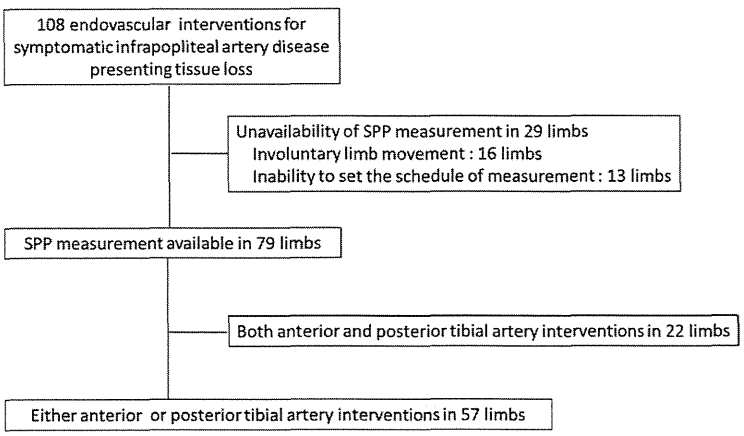

Figure 1. A flow diagram of the subjects included in this study. SPP indicates skin perfusion pressure.

Table 1. Baseline Characteristics of the Study Subjects

Patients, n	44
Age, y; median, interquartile range	71, 66–76
Men, n (%)	34 (77)
Hypertension, n (%)	37 (84)
Dyslipidemia, n (%)	20 (45)
Diabetes mellitus, n (%)	33 (75)
History of smoking, n (%)	32 (73)
End-stage renal disease, n (%)	23 (52)
Coronary artery disease, n (%)	22 (50)
Heart failure, n (%)	20 (45)
Limbs, n	57
Dorsal skin perfusion pressure, mm Hg; median, interquartile range	31, 22–40
Plantar skin perfusion pressure, mm Hg	31.2±14.5
Ankle-brachial index	0.72±0.38

Table 2. Summary of the Vessels Treated

	n
ATA system revascularization (n=40)	
ATA alone	37
ATA+DP artery	1
DP artery alone	2
Concomitant peroneal artery intervention	8
PTA system revascularization (n=17)	
PTA alone	16
PTA+plantar artery	1
Plantar artery alone	0
Concomitant peroneal artery intervention	3

ATA indicates anterior tibial artery; DP, dorsalis pedis; and PTA, posterior tibial artery.

P=0.616; Table 5). In the subgroup analysis of subjects with diabetes mellitus or end-stage renal disease, similar findings were observed in change in SPP and ΔSPP (Tables 6 and 7). Post-SPP and ΔSPP were higher on the dorsal (direct intervention) side than on the plantar (indirect intervention) side, as predicted by the recent 2D angiosome theory, in only 64% and 58% of patients, respectively. Correcting for autocorrelation between participant's subjects and limbs in a mixed model with a random intercept yielded similar results (Tables 8–11).

With PTA revascularization, dorsal SPP increased significantly from 29.3±14.0 to 42.4±19.7 mm Hg (P=0.003) after indirect intervention and plantar SPP increased significantly from 29.3±9.8 to 43.5±15.9 mm Hg (P<0.001) after direct intervention (Table 4). Also, there were no significant differences in both pre-SPP and post-SPP between the dorsal (indirect intervention) side and the plantar (direct intervention) side. ΔSPP was comparable between the dorsal (indirect intervention) side and the plantar (direct intervention) side (13.1±14.6 versus 14.1±11.4 mm Hg; P=0.833; Table 5). In the subgroup analysis of subjects with diabetes mellitus or end-stage renal

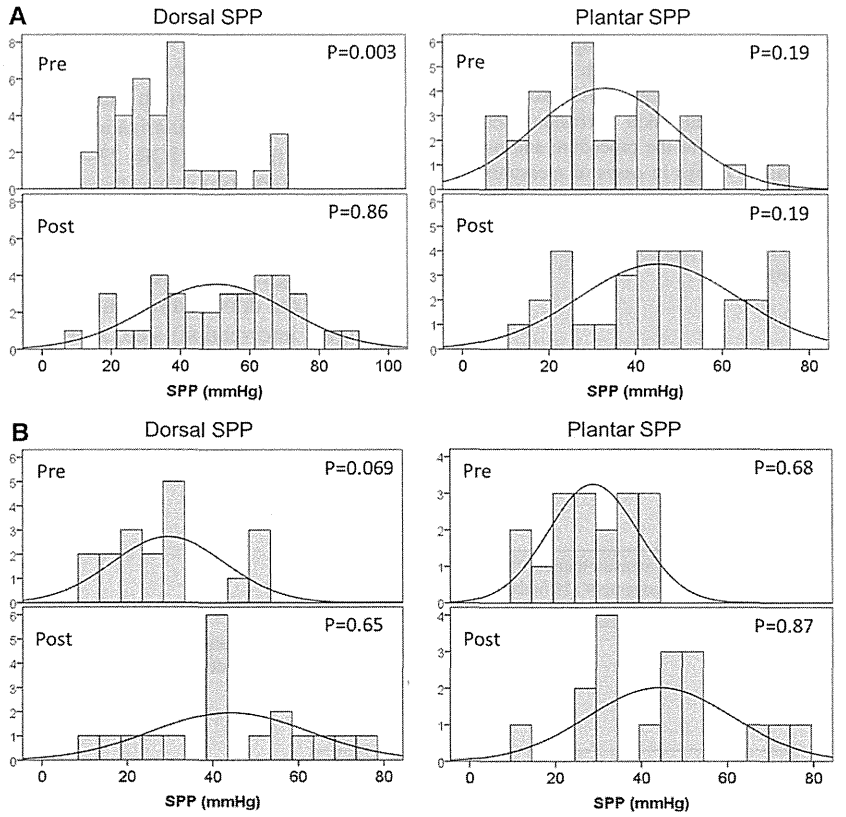

Figure 2. Skin perfusion pressure (SPP) distribution before and after anterior tibial artery revascularization (**A**) and posterior tibial artery revascularization (**B**). *P* value for the Shapiro–Wilk test.

Table 3. Postintervention Angiographic Findings

	Anterior Tibial Artery Intervention (n=40)	Posterior Tibial Artery Intervention (n=17)	*P* Value
No. of run-off vessels	1.9±0.7	1.5±0.6	0.129
Patent peroneal artery	26 (65%)	10 (59%)	0.767
Patent pedal arch	18 (45%)	6 (35%)	0.567

Patent was defined as the absence of significant stenosis (≥50% stenosis).

disease, similar findings were observed in change in SPP and ΔSPP (Tables 6 and 7). Post-SPP and ΔSPP were higher on the plantar (direct intervention) side than on the dorsal (indirect intervention) side, as predicted by the recent 2D angiosome theory, in only 47% and 40% of patients, respectively. Correcting for autocorrelation between participant's subjects and limbs in a mixed model with a random intercept yielded similar results (Tables 8–11).

About clinical outcomes, during the mean follow-up of 17±11 (range, 1–33) months, the complete wound healing rate was 52.6% and the major amputation rate was 3.5%. Healed limbs had higher post-SPP values (dorsal, 50.0±18.4; plantar, 45.9±17.6 mm Hg) than nonhealed limbs (dorsal, 46.8±21.1; plantar, 42.6±19.1 mm Hg), but this difference was not statistically significant (Table 12). In addition, post-SPP values were significantly higher in healed limbs with PTA intervention (dorsal, 54.6±18.4; plantar, 54.6±12.1 mm Hg) when compared with that in nonhealed limbs (dorsal, 33.0±15.8; plantar, 33.8±12.3 mm Hg; Table 12). Correcting for autocorrelation between participant's subjects and limbs in a mixed model with a random intercept yielded similar results (Table 13).

Table 4. SPP and Ankle-Brachial Index Before and After Intervention

	Pre	Post	*P* Value	Difference	95% CI
Anterior tibial artery revascularization					
Dorsal SPP, mm Hg (direct intervention)	Median, 33; IQR, 23–40.5	Median, 52; IQR, 32.5–65	<0.0001*†	15.48	9.52 to 21.43
Plantar SPP, mm Hg (indirect intervention)	31.6±16.1	44.8±19.2	0.001†	13.17	5.96 to 20.37
Ankle-brachial index	0.74±0.38	0.87±0.24	0.066	−0.13	−0.26 to 0.00
Posterior tibial artery revascularization					
Dorsal SPP, mm Hg (indirect intervention)	29.3±14.0	42.4±19.7	0.003†	13.13	5.34 to 20.91
Plantar SPP, mm Hg (direct intervention)	29.3±9.8	43.5±15.9	<0.001†	14.13	7.81 to 20.45
Ankle-brachial index	0.64±0.37	0.80±0.36	0.271	−0.16	−0.47 to 0.15

CI indicates confidence interval; IQR, interquartile range; and SPP, skin perfusion pressure.

*Wilcoxon signed-rank test.

†*P* value after Bonferroni correction: <0.0083.

Table 5. ΔSPP Before and After Intervention

	ΔSPP on the Dorsal Side, mm Hg	ΔSPP on the Plantar Side, mm Hg	*P* Value	Difference	95% CI
Anterior tibial artery revascularization	15.5±18.6 (direct intervention)	13.2±21.3 (indirect intervention)	0.616	3.63	−2.93 to 10.18
Posterior tibial artery revascularization	13.1±14.6 (indirect intervention)	14.1±11.4 (direct intervention)	0.833	0.13	−9.02 to 9.27

CI indicates confidence interval; and SPP, skin perfusion pressure.

Discussion

To the best of our knowledge, this study is the first to highlight the effects of single tibial artery revascularization based on assessments of dorsal and plantar microcirculation in relation to the recent concept of the 2D angiosome. The main findings of this study are (1) both dorsal and plantar SPP increased significantly after single tibial artery revascularization of either the ATA or the PTA, (2) both ATA and PTA revascularization were not significantly associated with differences in ΔSPP between the dorsal and the plantar foot, and (3) approximately half of the revascularized feet had changes in SPP that do not correspond to the recently defined 2D angiosome theory.

In the fields of bypass surgery and endovascular therapy, an emphasis on angiosome-oriented revascularization was adopted in the context of limb salvage and wound healing, despite a lack of randomized studies.[8–10] In the middle of the current 2D angiosome boom, more recent studies have raised objections to this approach that sounds good in theory.[11–13]

Table 6. SPP and Ankle-Brachial Index Before and After Intervention in Patients With Diabetes Mellitus or End-Stage Renal Disease

	Pre	Post	*P* Value	Difference	95% CI
Anterior tibial artery revascularization					
Dorsal SPP, mm Hg (direct intervention)	Median, 35; IQR, 28–41	Median, 52; IQR, 38–65	0.0001*†	14.32	8.31 to 20.34
Plantar SPP, mm Hg (indirect intervention)	31.7±15.9	44.9±19.2	0.001†	13.18	5.48 to 20.88
Ankle-brachial index	0.75±0.39	0.87±0.25	0.089	-0.12	−0.26 to 0.02
Posterior tibial artery revascularization					
Dorsal SPP, mm Hg (indirect intervention)	Median 27, IQR, 21–33	Median 42, IQR, 31–56	0.0506*	13.11	2.31 to 23.92
Plantar SPP, mm Hg (direct intervention)	26.4±10.3	38.2±13.5	0.004†	11.78	4.84 to 18.71
Ankle-brachial index	0.58±0.48	0.68±0.33	0.690	−0.09	−0.64 to 0.45

CI indicates confidence interval; IQR, interquartile range; and SPP, skin perfusion pressure.

*Wilcoxon signed-rank test.

†*P* value after Bonferroni correction: <0.0083.